FEATURE ARTICLE

Oxide- and Zeolite-Supported Molecular Metal Complexes and Clusters: Physical Characterization and Determination of Structure, Bonding, and Metal Oxidation State

Juan C. Fierro-Gonzalez, Stefan Kuba, Yalin Hao, and Bruce C. Gates*

Department of Chemical Engineering and Materials Science, University of California, Davis, California 95616

Received: December 6, 2005; In Final Form: April 2, 2006

This article is a review of the physical characterization of well-defined site-isolated molecular metal complexes and metal clusters supported on metal oxides and zeolites. These surface species are of interest primarily as catalysts; as a consequence of their relatively uniform structures, they can be characterized much more precisely than traditional supported catalysts. The properties discussed in this review include metal nuclearity, oxidation state, and ligand environment, as well as metal−support interactions. These properties are determined by complementary techniques, including transmission electron microscopy; X-ray absorption, infrared, Raman, and NMR spectroscopies; and density functional theory. The strengths and limitations of these techniques are assessed in the context of results characterizing samples that have been investigated thoroughly and with multiple techniques. The depth of understanding of well-defined metal complexes and metal clusters on supports is approaching that attainable for molecular analogues in solution. The results provide a foundation for understanding the more complex materials that are typical of industrial catalysts.

1. Introduction

Metal complexes and clusters dispersed on high-area metal oxide and zeolite supports are important industrial catalysts, exemplified by metallocenes on silica for alkene polymerization[1] and platinum clusters on zeolite LTL for naphtha dehydrocyclization.[2,3] When the supported catalytic species are uniform, they are regarded as molecular analogues, with structures that may be determined far more precisely than those of typical supported metal catalysts consisting of particles (or crystallites) of metal on supports (these are referred to as conventional supported metals in this review), which are notoriously heterogeneous.

Mononuclear metal complexes (with single metal atoms) and metal clusters (with more than one metal atom) have been synthesized on numerous supports, often from molecular precursors with highly reactive ligands, typified by organometallic compounds. Typically, the surface areas of the supports are of the order of 100 m^2/g, and the metal loadings are in the range of 0.5−3.0 wt %, with a typical value of 1.0 wt %; these values roughly match those of most supported metal catalysts used in industry. These metal loadings are low enough that the supported species are often sufficiently separated from each other to give structures that act almost independently of each other.

In contrast to industrial catalysts, which are made from salt precursors and are less than well defined structurally, the samples considered here are typically prepared by bonding of metal-complex or cluster precursors to the support, followed by treatments to modify their ligands without changing the number of metal atoms in the supported species. (Supported molecular metal complexes prepared in this way are often referred to as anchored metal complexes.) Thus, the precursors may be mononuclear metal complexes, typified by $Rh(CO)_2$(acac) (acac is $CH_3COCHCOCH_3$), or metal clusters, typified by $Rh_6(CO)_{16}$. In the preparation, sintering and fragmentation of the metal on the support are to be avoided.

When they have high degrees of uniformity, supported catalysts that are virtually molecular in character are subject to much more incisive structural characterization than the typically nonuniform conventional supported catalysts. Supported molecular catalysts also offer in prospect the practical advantages of molecular catalysts in solution (high selectivity and uniform accessibility), combined with the advantages of solid catalysts generally (ease of separation from products, lack of corrosiveness, and, in favorable cases, robustness for operation at high temperatures).

Consequently, researchers have dedicated substantial effort to the development of methods for synthesis and characterization of supported molecular metal complexes and clusters. The following review is a summary illustrating the methods that we judge to be most effective for characterization of such materials. The chemistry of synthesis of these materials has been reviewed[4−8] and is addressed only briefly here. The supports considered in this review are high-area porous oxides and zeolites, which are the supports of most practical importance in catalysis. (Metal clusters and particles on low-area supports such as single crystals constitute a well-developed subject in their own right, but for the most part they require experimental methods different from those considered here, as summarized in recent reviews,[9,10] and we barely mention them.)

We summarize the characterization of virtual molecular metal complexes and clusters on supports, focusing on the metal oxidation states and the structure and bonding of the supported species, including the ligands bonded to the metals and the metal−support bonding. Because the structures of catalysts

* To whom correspondence should be addressed. E-mail: bcgates@ucdavis.edu. Fax: (530) 752-1031.

10.1021/jp0571123 CCC: $33.50
Published on Web 06/17/2006

Juan C. Fierro-Gonzalez was born in 1978 in Toluca, Mexico. He graduated from Universidad Autonoma de San Luis Potosi in 2001, obtaining the highest score in the national exam for chemical engineers in Mexico (EGEL-IQ). He joined Prof. Bruce Gates' research group at the University of California, Davis, in 2001, and worked in a collaborative research project with people from the U. S. and South Africa, sponsored by NSF. His doctoral work was focused on the role of the oxidation state(s) of gold on the activity of supported gold complexes and nanoclusters for CO oxidation catalysis. He obtained his PhD degree in 2005 and is now a professor in the Department of Chemical Engineering at Instituto Tecnológico de Celaya in Mexico.

Stefan Kuba attended schools in Bavaria and Paris and studied at the Ludwig-Maximilians-Universität in Munich, earning his doctorate in physical chemistry in 2002 in the group of Professor Helmut Knözinger. He did further research in Knözinger's group and in the groups of Professor Michel Che at the University Pierre et Marie Curie in Paris and Professor Bruce Gates at the University of California, Davis. In 2003 he continued research in the Gates group with support from a Feodor Lynen Fellowship of the Alexander von Humboldt Foundation. His research focus has been on surface physical chemistry and spectroscopy, with an emphasis on characterization and testing of solid−acid and supported noble metal cluster catalysts. Since 2004, Dr. Kuba has done intellectual property work at the firm of Schwabe−Sandmair−Marx in Munich.

typically depend on the reactants in contact with them, we address methods that apply to samples in reactive atmospheres.

Our goal is to provide an assessment of the methods for characterization of well-defined supported metal-complex and metal-cluster catalysts, with examples showing the strengths and limitations of the methods and how they complement each other. Characterization of surface species consisting of only one or a few atoms is challenging, because these species are small, dispersed, and potentially nonuniform; as a rule, more than one technique is needed to determine structures with some confidence. We emphasize that by representing the supported species as uniform molecular analogues, we usually neglect the intrinsic nonuniformity of the sites on the support surfaces, and thus the corresponding variations in structure and bonding of the supported species. Because of this lack of uniformity of the supports, the anchored materials are generally not characterizable by crystallographic methods such as X-ray diffraction. Instead,

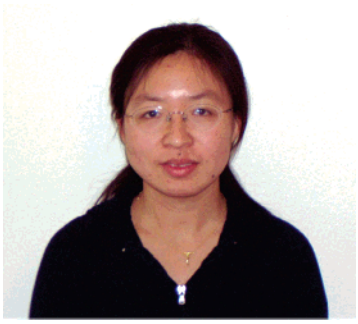

Yalin Hao graduated from Tianjin University (China) in 1997 with a B.S. degree in biochemical engineering. She joined Prof. Amyn Teja's research group at the Georgia Institute of Technology in 1999, working on the hydrothermal synthesis of iron oxide and cobalt oxide nanoparticles, obtaining her M.S. degree in chemical engineering in 2002. She is currently a Ph.D candidate at the University of California, Davis, in Prof. Bruce Gates' group. Her research, supported by DOE's Office of Basic Energy Sciences, is focused on the synthesis, testing, and characterization of supported metal complex and metal cluster catalysts with essentially molecular properties.

Bruce Gates is Distinguished Professor of Chemical Engineering at the University of California, Davis, where his group investigates the synthesis, spectroscopic and microscopic characterization, and catalytic testing of supported metal complexes and clusters. Gates is the author of *Catalytic Chemistry* (Wiley, 1992) and a coauthor of *Chemistry of Catalytic Processes* (McGraw-Hill, 1979). He edits the series *Advances in Catalysis* and co-edited *Metal Clusters in Catalysis* and *Surface Organometallic Chemistry: Molecular Approaches to Surface Catalysis.* He is a Director of the North American Catalysis Society and serves on DOE's Basic Energy Sciences Advisory Committee.

the most appropriate methods are those characterizing local surface structure and bonding, including (a) transmission electron microscopy (TEM); (b) a set of spectroscopic methods, including X-ray absorption (comprising extended X-ray absorption fine structure (EXAFS) and X-ray absorption near edge structure (XANES)), NMR, infrared (IR), Raman, Mössbauer, UV-visible, and others; (c) temperature-programmed methods such as reduction, oxidation, and decomposition; and (d) theory. These methods are developing rapidly, and results emerging from investigations of structurally simple samples such as the ones reviewed here are providing an important segment of the foundation for their improvement.

This review is not exhaustive; the techniques are presented only briefly, with guidelines about their application to supported metal-containing species. The examples are limited to relatively well-characterized samples that illustrate the techniques and how they complement each other. The review is organized as follows: (a) a brief introduction of sample handling for various characterization techniques; (b) a section about the number of metal atoms comprising the supported species (their nuclearities), followed by sections concerned with (c) the determination of oxidation states of metals in supported species; (d) ligands other than the support that are bonded to the metal; and (e)

metal−support interactions (with emphasis on the representation of the support as a ligand bonded chemically to the metal). The methods are illustrated with examples, and results summarized in figures show structural models with indications of the properties determined with various methods. Thus, some examples are considered repetitively in separate sections, with evidence being built up in steps regarding nuclearity, metal oxidation state, ligands, and supports. Some of the figures are intended to illustrate the complementary nature of the characterization methods and give an indication of which methods are most valuable for samples of various types.

2. Sample Handling and Limitations Imposed by Specific Characterization Techniques

Because the supports used to synthesize the samples are high-area metal oxides and zeolites of the kind used in practical catalysts, the samples are in the form of powders. The various characterization methods considered here impose a range of constraints on the handling of the samples. Often, because they react with O_2 or moisture, the samples need to be handled in the absence of air. For example, air-sensitive samples may be prepared under dry N_2 in a glovebox and then transferred in the absence of air to the equipment where characterization experiments are to be done. The sample handling requirements depend on the characterization techniques, and so the following section provides a summary of the restrictions imposed on the forms of the samples and their handling by the techniques considered here.

Although our goals do not include descriptions or evaluations of the techniques, we provide details of these in the cases for which they are not widely accessible.

TEM. For TEM, holey carbon grids with diameters of typically 3 mm are dipped into the powder sample (typically, a few milligrams) and then transferred to a sample holder. In the resultant samples, powder particles adhere to the carbon, and often the best measurements are made of particles dangling over the edges of the carbon. Samples are usually exposed to air while being mounted in the sample holder, but devices for handling air-sensitive samples for TEM are available.[11]

IR Spectroscopy. For IR spectroscopy, about 0.05 g of sample is typically needed for characterization either by transmission or diffuse reflectance spectroscopy. For transmission spectroscopy, the samples are pressed into wafers and typically placed between KBr windows or mounted in a frame that may allow their transfer to various positions in a cell, allowing recording of spectra or treatment under vacuum or in gas atmospheres.[12] For diffuse reflectance spectroscopy, powders can be used, and these may be the same as the samples used for conventional measurements of catalyst performance.

IR spectra can be recorded with the samples under vacuum or in reactive atmospheres, which may be flowing gases; flow experiments are advantageous, because changes in properties can be determined not only as a function of time, but, in prospect, in a steady state. If the sample is characterized in a reactive atmosphere, powders are preferred over wafers to reduce the resistance to mass and heat transport and thereby to minimize the gradients in concentration and temperature; such gradients are undesirable because they give nonuniform samples and complicate the interpretation of spectra. These transport issues pertain as well to all the spectroscopic techniques used to characterize samples in reactive atmospheres. Wafers that are thin enough to be characterized by negligible gradients are often sufficient to give high-quality spectra. Regardless of the mode of spectroscopy that is used, numerous scans are usually averaged to provide an IR spectrum of high quality; Fourier transform spectrometers are advantageous in this regard and almost always used. More scans are needed when a sample is in a reactive atmosphere than when it is under vacuum, because the gases may absorb some radiation. Therefore, it is advantageous to use cells with small dead volumes and spectrometers that have evacuated sample chambers for mounting of the cell. The presence of an atmosphere requires subtraction of the background that it contributes to the spectrum. Numerous cells for transmission[13,14] and for diffuse reflectance spectroscopy[13] have been reported, including some that are flow reactors as well as cells.

Raman Spectroscopy. For Raman spectroscopy, typically, 0.05 g of sample is needed. Sample preparation is easier than for IR spectroscopy because the sample can always be used in the form of a powder. Raman spectroscopy is especially powerful for samples in reactive atmospheres, as scattering from the reactant gases is usually negligible. Furthermore, glass Raman cells are easily constructed, and glass offers the advantage of being a weak Raman scatterer. With the use of a quartz reactor, Raman spectroscopy can be used to characterize catalysts working at temperatures of hundreds of degrees K.[15−18]

UV-Visible Spectroscopy. The amount of sample needed for UV-visible spectroscopy is similar to that needed for IR and Raman spectroscopies. UV-visible spectra of supported metals cannot usually be recorded in transmission because the samples are usually opaque, and scattering losses are high.[19] Therefore, experiments are normally done in diffuse reflectance mode. Cell designs are often simple and may allow gas streams to flow over the sample.[20]

NMR Spectroscopy. In solid-state NMR spectroscopy, the spectra are usually recorded under conditions of magic angle spinning (MAS), to remove the chemical shift anisotropy and some dipolar interactions. Proton dipolar couplings to rare spins (e.g., ^{13}C) are removed by strong decoupling fields. The procedure requires a sample rotor that can be spun at several thousand rotations per second. Samples are packed uniformly in the rotor to ensure stable spinning. The required mass of sample depends on the element being investigated and its concentration in the sample, typically being in the range of 0.05 to 0.4 g.

NMR characterization of samples under reaction conditions is fraught with challenges because of the need for spinning. There is a lack of cell designs that allow the recording of spectra with simultaneous spinning and gas flow. Usually, reactant gases are first brought into contact with the catalyst at low temperatures, and then the spectra are recorded at different temperatures with the rotor sealed.[21] In a more recent design, the reactant gases are first brought into contact with the catalyst at the desired temperature before the reactor is cooled rapidly by liquid nitrogen.[22] This so-called pulse-quench catalytic reactor allows a close approach to investigation of catalysts in the working state.

X-ray Absorption Spectroscopy (XAS). The mass of sample needed to record high-quality X-ray absorption spectra depends on the absorber metal in the sample and its loading. As a rule of thumb, in transmission mode this mass is calculated to yield an optimal absorption (i.e., a total absorbance of about 2.0 ± 0.5) at a given absorption edge. Typically, the amount of sample (with a loading of a second- or third-row transition metal of approximately 1 wt %) ranges from approximately 0.1 to 0.6 g.

The spectra can be recorded either in transmission or fluorescence mode. The preferred mode depends on the

TABLE 1: Examples of Metal Edges and Scan Modes Commonly Used in X-ray Absorption Spectroscopy for Various Metal−Support Combinations

sample	edge	energy, eV	scan mode
Au/MgO	Au L_{III}	11919	transmission
Au/zeolite NaY	Au L_{III}	11919	transmission
Au/TiO_2	Au L_{III}	11919	fluorescence
Au/La_2O_3	Au L_{III}	11919	fluorescence
Au/CeO_2	Au L_{III}	11919	fluorescence
Ir/γ-Al_2O_3	Ir L_{III}	11215	transmission
Ir/MgO	Ir L_{III}	11215	transmission
Ir/zeolite NaY	Ir L_{III}	11215	transmission
Ir/zeolite NaX	Ir L_{III}	11215	transmission
Os/MgO	Os L_{III}	10871	transmission
Re/MgO	Re L_{III}	10535	transmission
Re/γ-Al_2O_3	Re L_{II}, L_{III}	11959, 10535	transmission
Rh/γ-Al_2O_3	Rh K	23220	transmission
Rh/MgO	Rh K	23220	transmission
Rh/DAY zeolite	Rh K	23220	transmission
Rh/TiO_2	Rh K	23220	transmission
Rh/La_2O_3	Rh K	23220	transmission/fluorescence

combination of the support and metal and also on the edge(s) of the metal to be scanned (Table 1). Fluorescence is used when the support absorbs substantial radiation at the edge energy selected or when the metal loading is low. There is no rule for how low the metal loading has to be for fluorescence to be preferred, and experimenters rely on experience to decide which mode is best. However, fluorescence should be avoided if the metal loading is not too low because transmission would provide higher-quality spectra. More importantly, high metal loadings could lead to significant self-absorption or saturation in fluorescence measurements.

Transmission measurements are made with pressed wafers of sample or with powders packed into a tube or channel; fluorescence measurements are made with powders. In a transmission experiment, the complete thickness of the wafer or bed of sample through which the X-ray beam penetrates is characterized. Thus, homogeneity in the wafers or beds of particles is required. Variations in the thickness can introduce nonlinear responses in the spectra.[23] Because beds of particles are typically less uniform than pressed wafers, the quality of data obtained with the former is usually less than that obtained with the latter. In a fluorescence experiment, only a layer of powder with a thickness of about 5 μm is characterized, and thus only a few milligrams of sample may be sufficient.

Characterization of samples in the presence of flowing fluids may be affected by mass transfer limitations that result in concentration gradients, which could affect not only the performance of a sample as a catalyst but also its structure. Thus, cells[24−28] designed to contain samples in the form of powder (possibly serving as plug flow reactors) are appropriate, but it is essential that the concentration gradients resulting from the occurrence of the catalytic reaction not be too great—often it is good to use a "differential" reactor, with a low conversion. To provide insight into structural changes occurring in samples during reactions, the cells should allow data collection in the presence of gases with flow rates that are typical of the application of interest or can be applied for measurement of kinetics of the reaction. This requirement affects the dimensions of the cells, including the path length through the sample (which dictates in part the amount of absorbed radiation), thereby influencing the quality of the spectra.

X-ray absorption spectra of samples are usually recorded together with X-ray absorption spectra of a reference compound (e.g., a metal foil) placed in tandem with the sample in the X-ray beam to calibrate the energy of the absorption edge.

Replicate spectra are usually averaged in the analysis of XAS data. Because the quality of spectra recorded in transmission is generally higher than that of spectra recorded in fluorescence, more spectra usually are needed in fluorescence XAS.[29] Some details of XAS are given in the Appendix.

Temperature-Programmed Methods. Temperature-programmed decomposition (TPDE), temperature-programmed reduction (TPR), and temperature-programmed oxidation (TPO) may provide quantitative information that complements the information provided by spectroscopic techniques.

The mass of sample used in these temperature-programmed experiments is typically in the range from about 0.05 to 0.5 g. The samples are typically loaded into quartz reactors, where they are treated in flowing gases at increasing temperatures. In TPDE, the samples are usually treated in flowing He as the temperature increases linearly with respect to time. A thermal conductivity detector (TCD) is used for a quantitative measure of the formation of gases (such as CO and H_2) formed from the sample, and these measurements are often accompanied by mass spectrometric identification of the gases.[35,36] In TPR or TPO experiments, the samples are treated with reducing (e.g., H_2, CO) or oxidizing (e.g., O_2) gases, respectively. The data are usually presented as temperature profiles showing peaks representing the evolution (or consumption) of gases, and integration based on data obtained with standard materials is used for quantification. As a rule, samples with relatively simple and nearly uniform structures lead to sharper peaks than samples consisting of complex, nonuniform structures.

3. Nuclearity of Metal Species (EXAFS, IR, and Raman Spectroscopies; TEM; DFT)

Methods such as TEM are among the most informative for determining the sizes of small supported species, because the information is available directly in images. TEM imaging of single metal atoms on a support is still so challenging that only a few examples have been reported, and we know of no reports of isolated supported metal complexes that have been imaged. In contrast, clusters of several atoms of a heavy metal are large enough to be imaged by many high-resolution TEM instruments, and a number of examples have been reported.[11,37−39]

In the absence of images of the supported species, evidence of metal nuclearity often has to be inferred from spectroscopic data. EXAFS spectra are among the most useful in this regard, because they provide metal−metal coordination numbers. Interpretation of EXAFS data is subtle and based on data fitting, and details are provided below.

Metal−metal bonds in some supported clusters can be characterized by Raman spectroscopy, and indirect evidence of the presence of metal clusters can also be obtained from other spectra characterizing cluster−ligand combinations; for example, bridging CO ligands indicate metal−metal bonds and hence metal clusters.

In general, successful characterization of a supported metal complex or cluster requires a combination of techniques, and one of our major goals is to illustrate how the available techniques complement each other. We begin by considering the smallest supported species, mononuclear metal complexes, followed by ensembles of these complexes (which lack metal−metal bonds), and then metal clusters (species with metal−metal bonds).

A. Mononuclear Metal Complexes and Ensembles of these Complexes. Supported species consisting of only single metal atoms combined with ligands—site-isolated mononuclear metal complexes—are characterized by EXAFS first-shell metal−metal coordination numbers indistinguishable from zero. When samples contain metals with near-neighbor metal centers, EXAFS spectra

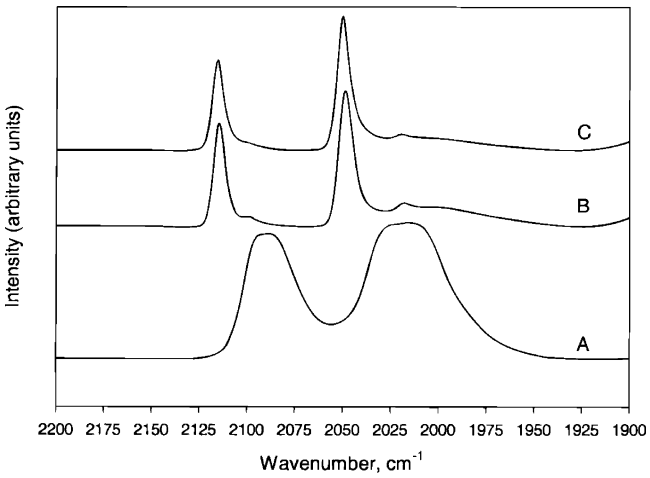

Figure 1. IR spectra in the ν_{CO} stretching region of zeolite Y-supported $Rh(I)(CO)_2$: (A) support was zeolite NaY calcined at 473 K; (B) support was DAY zeolite calcined at 393 K; and (C) support was DAY zeolite calcined at 573 K.[40] From ref 40, used with permission.

indicate nonzero metal−metal coordination numbers and thus a basis for estimation of the nuclearity. Such samples include both ensembles of metal complexes and metal clusters.

A simple supported mononuclear metal complex on a nearly uniform (crystalline) support is $Rh(CO)_2$ on dealuminated Y zeolite (DAY zeolite).[40] This sample was formed by the reaction of $Rh(CO)_2(acac)$ in a *n*-hexane slurry with the zeolite. The supported species is identified as mononuclear, in part because EXAFS data measured in transmission mode at the Rh K edge show a Rh−Rh coordination number indistinguishable from zero.

The interpretation of a metal−metal coordination number indistinguishable from zero as an indication of the lack of metal−metal shells is influenced by the errors introduced during the experiments and the data analysis. Errors in the EXAFS measurements include both statistical and systematic contributions. The former errors arise from photon-counting statistics, electronic noise, fluctuations in the position of the X-ray beam, and other sources. As they vary randomly in sign and magnitude, these errors can be minimized by averaging several scans or by using longer integration times. Systematic errors can be introduced both during spectrum acquisition and data analysis. Some acquisition-related sources of systematic errors, such as sample inhomogeneities, improper cell alignment, and insufficient suppression of higher harmonics, can be nearly eliminated by application of good experimental techniques. However, a number of substantial systematic errors introduced during the data analysis are unavoidable.[41] EXAFS data are analyzed in a fitting process, involving comparisons of data with data characterizing reference materials and/or predictions based on theory. The appropriate choice of reference compounds to provide a basis for fitting the various absorber−backscatterer contributions is especially important. References can be obtained from experimental results recorded for known compounds or from theoretical calculations done with the FEFF code.[30] In both cases, the compound that is chosen as the reference should have a structure that is as similar as possible to that expected for the sample to be analyzed. If the reference is experimental, EXAFS spectra of both the reference compound and the sample to be analyzed should be recorded under similar conditions. Other systematic errors may arise in the analysis during background removal, normalization, and Fourier transformation of the data. Because there is such a variety of sources of errors associated with EXAFS spectroscopy, errors propagated into the structural parameters determined in the fitting are not easily quantified. Typically, errors in the values of coordination numbers and distances representing metal−metal contributions are estimated to be about ±10% and 0.02 Å, respectively.[42]

Low-Z scatterers (carbon, oxygen, or aluminum atoms, for example) around an absorbing metal atom can also be identified by EXAFS spectroscopy (Table 2), with the data providing information about the coordination of the metal in the supported species; such information can sometimes be used indirectly to characterize the metal nuclearity. However, the errors in the

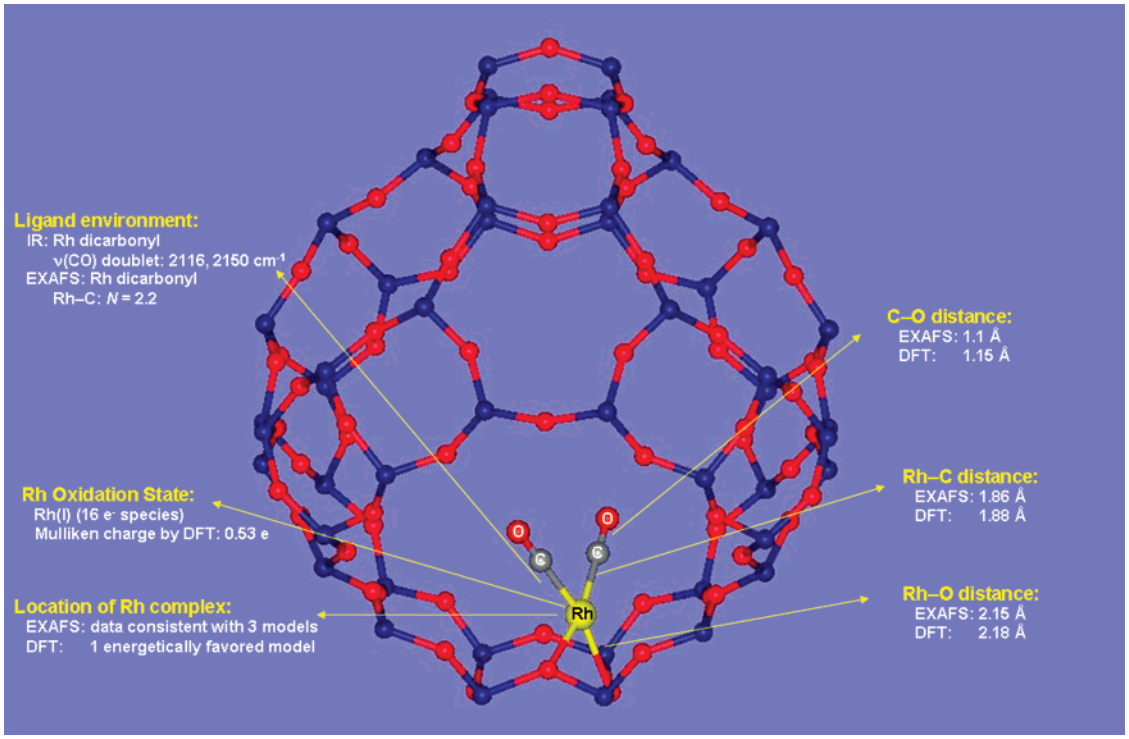

Figure 2. Structural model of zeolite Y-supported $Rh(I)(CO)_2$ derived from IR and EXAFS characterization and DFT calculations.[40]

TABLE 2: Summary of Isolated Supported Mononuclear Metal Complexes with Structures Determined by EXAFS Spectroscopy[a]

				M−ligand contributions							
				M−$O_{support}$		M−C		M−O*			
support	precursor	formal oxidation state of metal in precursor	method of preparation	*N*	*R*, Å	*N*	*R*, Å	*N*	*R*, Å	model of surface species	ref
MgO calcined at 673 K	$Au(CH_3)_2(acac)$	3	adsorption from pentane	2.1	2.16	–	–	–	–	$Au(CH_3)_2\{OMg\}_2$	99
TiO_2 calcined at 673 K	$Au(CH_3)_2(acac)$	3	adsorption from pentane	2.1	2.15					$Au(CH_3)_2\{OTi\}_2$	111
zeolite NaY calcined at 573 K	$Au(CH_3)_2(acac)$	3	adsorption from pentane	1.9	2.08					$[Au(CH_3)_2(acac)]$ /zeolite NaY	158
La_2O_3 calcined at 673 K	$Au(CH_3)_2(acac)$	3	adsorption from pentane	2.1	2.15	0.4	1.84			$Au(CH_3)_2\{OLa\}_2$	103
γ-Al_2O_3 calcined at 673 K	$Os_3(CO)_{12}$	0	decarbonylation in He at 423 K followed by treatment with CO at 473 K	2.9	2.17	2.4	1.93	3.1	3.04	$Os(CO)_3\{HOAl\}_{3-x}\{OAl\}_x$ x = 0−3	159
γ-Al_2O_3 calcined at 673 K	$Os(CO)_3\{HOAl\}_{3-x}\{OAl\}_x$, x = 0−3	ca. 2	oxidative fragmentation in vacuum at 573 K	3.9	2.17	2.0	1.85	2.4	3.04	$Os(CO)_2\{HOAl\}_{4-x}\{OAl\}_x$ x = 0−4	159
γ-Al_2O_3 calcined at 673 K	$Os_3(CO)_{12}$	0	oxidative fragmentation in He at 423 K	3.0	2.17	2.8	1.91	2.8	3.05	$Os(CO)_x\{OAl\}_3$ (mixture of $Os(CO)_2$ and $Os(CO)_3$)	160
γ-Al_2O_3 calcined at 573 K	$Ru_3(CO)_{12}$	0	oxidative fragmentation in He at 423 K	1.8	2.17	1.8	1.9	2.0	2.97	$Ru(CO)_2\{OAl\}_2$	161
SiO_2 calcined at 433 K	$Ru_3(CO)_{12}$	0	oxidative fragmentation in air at 298 K	4.9	2.08	2.0	1.87	2.0	3.01	$Ru(CO)_2\{OSi\}_x$	162
γ-Al_2O_3 calcined at 433 K	$Rh_4(CO)_{12}$	0	oxidative fragmentation in air at 298 K	7.0	2.04	2.0	1.81	2.0	3.00	$Rh(CO)_2\{OAl\}_x$	162
DAY zeolite calcined at 393 K	$Rh(CO)_2(acac)$	1	adsorption from hexane	1.8	2.16	2.3	1.86	2.2	2.97	$Rh(CO)_2\{OAl\}$ $\{OSi\}$	40
DAY zeolite calcined at 573 K	$Rh(CO)_2(acac)$	1	adsorption from hexane	1.9	2.15	2.2	1.86	2.3	2.96	$Rh(CO)_2\{OAl\}$ $\{OSi\}$	40
DAY zeolite calcined at 773 K	$Rh(C_2H_4)_2(acac)$	1	adsorption from pentane	2.2	2.19	3.9	2.09			$Rh(C_2H_4)_2\{OAl\}$ $\{OSi\}$	46
MgO calcined at 773 K	$Rh(C_2H_4)_2(acac)$	1	adsorption from pentane	1.4	2.18	4.0	2.04			$Rh(C_2H_4)_2\{OMg\}_x$	163
γ-Al_2O_3 not calcined	$RhCl_3$	3	reduction with H_2 at 593 K followed by interaction with CO at 298 K	3.1	2.12	1.8	1.80	1.8	3.00	$Rh(CO)_2\{OAl\}_x$	164
MgO calcined at 973 K	$HRe(CO)_5$	1	adsorption from hexane	no evidence of interaction		5.0	1.94	5.0	3.13	$HRe(CO)_5$ molecularly adsorbed complexes	165
MgO calcined at 973 K	$HRe(CO)_5$	1	decarbonylation with H_2 at 353 K	2.8	2.13	3.0	1.91	3.2	3.12	$Re(CO)_3\{HOMg\}_{3-x}\{OMg\}_x$ x = 0−3	165
MgO calcined at 673 K	$HRe(CO)_5$	1	decarbonylation with H_2 at 353 K	2.8	2.13	3.3	1.87	3.1	3.11	$Re(CO)_3\{HOMg\}_{3-x}\{OMg\}_x$ x = 0−3	166
MgO calcined at 663 K	$Re_4(CO)_{12}(OH)_4$	1	oxidative fragmentation in vacuum at 498 K	3.1	2.17	3.2	1.90	3.3	3.07	$Re(CO)_3\{HOMg\}_{3-x}\{OMg\}_x$ x = 0−3	130
MgO calcined at 663 K	$Re_2(CO)_{10}$	0	oxidative fragmentation in vacuum at 398 K	3.1	2.18	2.8	1.88	2.9	3.08	$Re(CO)_3\{HOMg\}_{3-x}\{OMg\}_x$ x = 0−3	130
MgO calcined at 523 K	$DRe(CO)_5$	1	decarbonylation with H_2 at 353 K	2.5	2.16	2.8	1.88	3.0	3.09	$Re(CO)_3\{HOMg\}_{3-x}\{OMg\}_x$ x = 0−3	130
MgO calcined at 523 K	$DRe(CO)_5$	1	exposure to CH_3OH-saturated He at 423 K	3.1	2.13	2.8	1.85	2.8	3.07	$Re(CO)_3\{HOMg\}_{3-x}\{OMg\}_x$ x = 0−3	130
SiO_2 calcined at 773 K	$Zr(Np)_4$ (Np = neopentyl)	4	adsorption from pentane	1.1	1.96	3.2	2.22	–	–	$Zr(Np)_3\{OSi\}$	140
SiO_2 calcined at 973 K	$Ta(=CHtBu)(Np)_3$ (Np = neopentyl)	5	adsorption from pentane	1 1	1.90 2.64	1 2	1.90 2.15	–	–	$Ta(=CHtBu)((Np)_2\{OSi\}$	137
SiO_2 calcined at 973 K	$Re(\equiv CtBu)(=CHtBu)(Np)_2$ (Np = neopentyl)	7	adsorption from pentane	1 1	2.02 2.42	2 1	1.79 2.01			$Re(\equiv CtBu)(=CHtBu)(Np)\{OSi\}$	136
SiO_2 calcined at 773 K	$Zr(Np)_3\{OSi\}$	4	treatment with H_2 at 423 K	3.1 1.1	1.95 2.61	–	–	–	–	$ZrH\{OSi\}_3$	140
SiO_2 calcined at 773 K	$Ta(=CHtBu)((Np)_2\{OSi\}$ and $Ta(=CHtBu)((Np)\{OSi\}_2$ (Np = neopentyl)	5	treatment with H_2 up to 498 K	2.3 0.7	1.89 2.63	–	–	–	–	$TaH\{OSi\}_2$	145

[a] Notation: *N*, coordination number; *R*, distance between absorber and backscatterer atoms. O* is carbonyl oxygen. Expected errors: *N*, ± 10%; *R*, ± 0.02 Å.

coordination numbers and interatomic distances characterizing these shells are typically larger than those characterizing the metal−metal contributions.

Generally, hydrogen atoms bonded to the metal cannot be identified by EXAFS spectroscopy. In principle, contributions from such small atoms are expected to be evident in the low-*r* portion of the Fourier transformed spectra and constitute the atomic X-ray absorption fine structure (AXAFS) (*r* is the distance from the absorber atom to a backscatterer atom). Hydrogen adsorbed on metal clusters leads to significant changes in the AXAFS spectra.[43−45]

The groups incorporating low-Z neighboring atoms are usually more efficiently characterized by other techniques, such as IR and NMR spectroscopies. For example, in the aforementioned sample prepared from $Rh(CO)_2(acac)$ and a zeolite, IR spectra demonstrated the presence of a zeolite-supported dicarbonyl of rhodium (Figure 1), with the symmetry inferred from the IR spectra demonstrating that the species was mononuclear, in agreement with the EXAFS results. Complementary evidence was provided by calculations based on theory at the density functional level, and the agreement between the calculated and experimental values provides a self-consistent foundation for the structural model (Figure 2).[40]

The fact that the support is crystalline (a zeolite) contributes to the relative uniformity of the sites; it has been suggested that most of the $Rh(CO)_2$ groups are present at crystallographically equivalent positions. The sharpness of the ν_{CO} IR spectra (Figure 1) suggests this near uniformity.[40] Evidence of the uniformity of zeolite-supported metal complexes can also emerge from NMR spectra, as exemplified by the ^{13}C NMR spectra of a DAY zeolite-supported rhodium-diethylene complex.[46] Similar to the DAY zeolite-supported $Rh(CO)_2$, the supported $Rh(C_2H_4)_2$ complex, formed from $Rh(C_2H_4)_2(acac)$, was characterized by EXAFS spectroscopy, which showed a Rh−Rh coordination number indistinguishable from zero. ^{13}C MAS NMR spectra of this supported complex after it had been exchanged with ethylene−$^{13}C_2$ were acquired over a range of temperatures (Figure 3). The ^{13}C resonance was broadened as a result of the conflict of $^1H-^{13}C$ dipolar decoupling and random anisotropic reorientation of the $^1H-^{13}C$ bond vector. The line width changed with the temperature, and, at a particular temperature, the resonance became undetectable, as it did in the precursor complex $Rh(C_2H_4)_2(acac)$ in the crystalline state. This result indicates that all the ethylene ligands in the sample were characterized by a common rotational barrier, which is extremely sensitive to the electronic and steric effects. Thus, it demonstrates the dynamic uniformity of the supported metal sites and, by inference, their structural uniformity.[46] As the structure is consistent with EXAFS and IR data as well as the ^{13}C NMR data, the result is believed to be the strongest demonstration of the virtual molecular character of any supported metal complex or cluster.

In contrast, the $Rh(C_2H_4)_2$ complex prepared similarly on the surface of MgO powder was not characterized by the disappearance of the ethylene resonance at any temperature, corresponding to the nonuniformity of the MgO surface sites and hence of the MgO-supported $Rh(C_2H_4)_2$ complexes.[46]

Another example of a supported mononuclear metal complex that has been characterized by a set of complementary techniques is a rhenium carbonyl bonded to MgO. This example affords a comparison with related samples that incorporate ensembles of such complexes.

Samples were synthesized from $HRe(CO)_5$ and from $H_3Re_3(CO)_{12}$; a goal was to use the former precursor to prepare isolated supported rhenium complexes and the latter to prepare ensembles of several such complexes, with the intent of determining how the catalytic properties depend on the nuclearity.[47−49] Evidence of the nuclearity is provided by EXAFS spectroscopy. The lack of detectable Re−Re contributions in the sample made from $HRe(CO)_5$ indicates the isolation of the rhenium complexes on the support, and, in contrast, the presence of Re−Re contributions (with a Re−Re first shell coordination number of 0.9) in the sample made from $H_3Re_3(CO)_{12}$ indicates neighboring rhenium centers, consistent with the presence of ensembles.

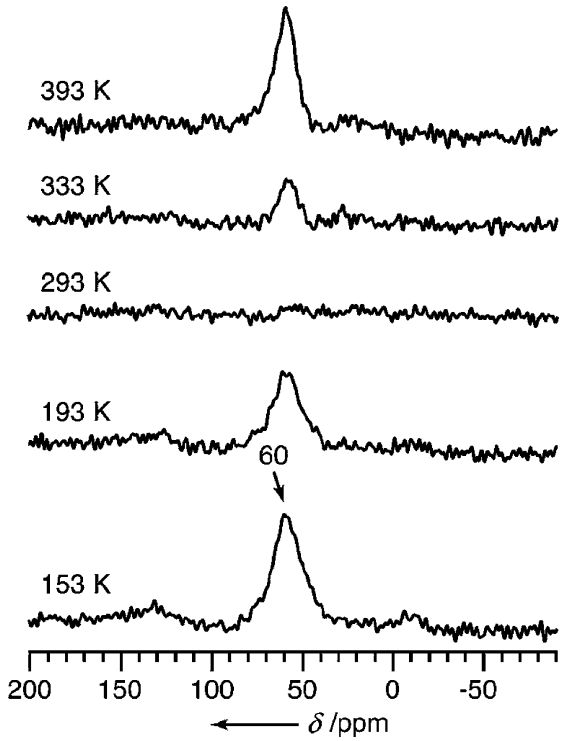

Figure 3. Variable-temperature ^{13}C MAS NMR spectra of ethylene $^{13}C_2$-exchanged $Rh(C_2H_4)_2$ supported on partially dehydroxylated zeolite DAY.[46] From ref 46, used with permission.

The data characterizing these samples give an indication of the value of applying complementary characterization techniques. For example, the IR spectra in the ν_{CO} region characterizing the sample made from $HRe(CO)_5$ support the inference that the rhenium was present in mononuclear complexes, as these spectra are similar to those of molecular analogues that are mononuclear; thus, the IR data complement the EXAFS data in pointing to such species.[47] Further support for the inference that the species are mononuclear rhenium carbonyls emerged from calculations at the density functional level, which were done (a) to evaluate the possibility of forming such complexes on the MgO surface, for which EXAFS and IR spectra provided some evidence, and (b) to estimate structural parameters (e.g., interatomic distances) and spectroscopic information (e.g., ν_{CO} frequencies) for the energetically favored structures.[50] The results of the calculations provide a basis for comparisons with the EXAFS and IR measurements.

Various structural models of the supported rhenium carbonyls were tested and optimized by energy minimization in the calculations, ruling out those for which discrepancies between the calculated structural parameters and the EXAFS and IR spectra were found. The best agreement between the calculations and the EXAFS and IR data led to the structural model shown in Figure 4. This model has the limitation that the representation of the MgO support may be a significant oversimplification,

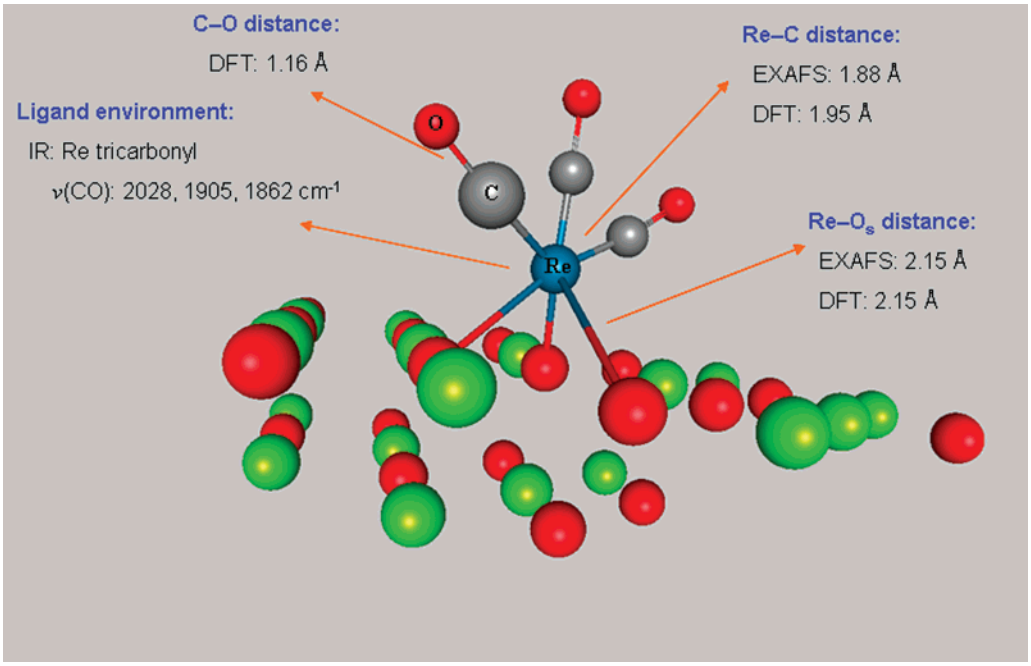

Figure 4. Structural model of rhenium carbonyl complexes on partially dehydroxylated MgO at a defect site, determined on the basis of EXAFS and IR spectra and DFT calculations.[47,50] From ref 50, used with permission.

because the surface of the powder support exposes various crystalline faces, and the metal complexes could be anchored to various sites. The simplification of the zeolite support structure in the model of the zeolite-supported $Rh(CO)_2$ complexes shown in Figure 2 is probably less severe than that of the MgO support used for the rhenium complex, because the zeolite is crystalline and more nearly uniform than the MgO. Further details of the supported rhenium structure are presented below.

In contrast to the sample prepared from $HRe(CO)_5$, the sample on the same support prepared from $H_3Re_3(CO)_{12}$ formed ensembles of rhenium complexes, again mononuclear, but in this sample located in near proximity to each other. Treatment of the sample synthesized by chemisorption of $H_3Re_3(CO)_{12}$ on the MgO support (giving $[H_2Re_3(CO)_{12}]^-$) in either He or H_2 at 498 K led to fragmentation of the metal frame of the supported clusters. The resultant species were characterized by IR spectra indicative of $Re(CO)_3$. Evidence of cluster fragmentation was provided by the lack of a Re−Re contribution in the EXAFS spectra at the Re−Re bonding distance of approximately 2.7 Å. Instead, a Re−Re contribution with a coordination number of 0.9 was found, with an average Re−Re distance of 3.94 Å (Table 3). The significance of this result is that it indicates the formation of ensembles of rhenium carbonyl complexes, which remained near each other on the support, as the metal frame of the trirhenium cluster precursor broke apart.[47] Catalytic reaction data[48,49] show that these ensembles were active for cyclopropane hydrogenolysis, whereas the sample made from $HRe(CO)_5$ and containing site-isolated rhenium complexes was inactive. This result provides further evidence of the neighboring metal centers in the former sample; this is one of only a few examples in which reactivity has been used as evidence of the nuclearity of supported species.

Ensembles of osmium complexes were prepared similarly by oxidative fragmentation of $Os_3(CO)_{12}$ adsorbed on MgO, and these have been characterized more incisively than the rhenium ensembles.[37] Exposure of the supported triosmium clusters to air led to their fragmentation and formation of ensembles of mononuclear osmium carbonyls, identified by IR spectroscopy

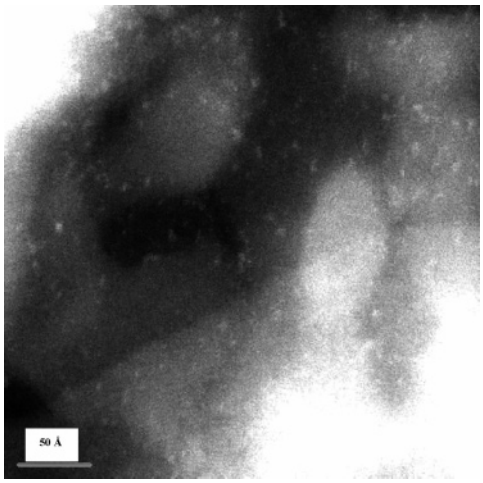

Figure 5. Z-contrast STEM image of sample formed from $Os_3(CO)_{12}$ supported on partially dehydroxylated MgO after treatment in air at room temperature for 1 h.[37] From ref 37, used with permission.

as principally $Os(CO)_2$. EXAFS spectra indicated an Os−Os coordination number of 2.0 (as in the precursor $Os_3(CO)_{12}$), with an average Os−Os distance of 3.33 Å (which is markedly greater than the Os−Os bonding distance in the precursor, 2.88 Å). These results are consistent with the formation of ensembles of three osmium carbonyl complexes on the support (Table 3).

Scanning transmission electron microscopy (STEM) images (Figure 5) confirm the presence of such ensembles, with the diameters of the observed scattering centers (6.0 Å) matching that indicated by the EXAFS results (6 Å), estimated on the basis of an atomic radius of Os of 1.33 Å combined with the assumption that the array was triangular.[37]

The STEM images provide evidence of the uniformity of the ensembles, and the agreement between the ensemble sizes determined by STEM and the average ensemble size determined by EXAFS spectroscopy provides a good confirmation of the value of EXAFS spectroscopy for characterization of such samples. In the absence of images, EXAFS data characterizing such structures are most incisive when the clusters or ensembles

TABLE 3: Summary of Supported Ensembles of Mononuclear Metal Complexes with Structures Determined by EXAFS Spectroscopy[a]

				M−M		M−O_s		M−ligand contributions: M−C		M−O*			
support	precursor	formal oxidation state of metal in precursor	method of preparation	*N*	*R*, Å	*N*	*R*, Å	*N*	*R*, Å	*N*	*R*, Å	model of surface species	ref
MgO calcined at 973 K	$H_3Re_3(CO)_{12}$	1	oxidative fragmentation in He or vacuum at 498 K	0.9	3.94	2.7	2.15	3.0	1.88	3.0	3.09	$Re(CO)_3\{OMg\}_3$ subcarbonyls not completely isolated from each other	47
MgO calcined at 673 K	$Os_3(CO)_{12}$	0	oxidative fragmentation by exposure to air for 6 h at 298 K	2.0	3.33	2.2	2.10	1.9	1.87	1.9	3.04	$Os(CO)_x\{OMg\}_2$ (mixture of $Os(CO)_2$ and $Os(CO)_3$), not completely isolated from each other	37

[a] Notation: same as in Table 2.

are small, highly symmetric, and uniform, but because EXAFS spectroscopy provides structural information that is averaged over the part of the sample that is probed by the incident X-rays, the results are often insufficient to distinguish the components of mixtures of similar species. The agreement between the EXAFS and STEM data in this example is important in demonstrating the relative uniformity of the supported species and thereby validating EXAFS spectroscopy as a basis for determining more than just the average nuclearity of the ensembles.

The STEM images do not incorporate enough structural information by themselves to determine the ensemble nuclearity, nor are they sufficient to determine the shapes of the ensembles, for various reasons. First, and most importantly, the individual metal atoms are not resolved in the STEM images. To allow atomic resolution, it would be necessary to achieve resolution at the sub-Angstrom scale. However, the spatial resolution is limited by the lens aberrations.[51] With recent advances in electron microscopy, this limitation can now be overcome by using aberration-corrected STEM. The improvement of the spatial resolution led to the successful imaging of metal atoms in platinum trimers[38] and trirhenium carbonyl clusters[39] supported on γ-Al_2O_3 discussed in the following section.

When atomic resolution is not attained, estimation of ensemble (or cluster) nuclearity from the apparent diameter determined from the images is possible, but the errors are substantial; for example, a discrepancy between the actual and apparent cluster size is caused by the Fresnel contrast effect at the surfaces of the clusters.[52] Another limitation of STEM is that the determination of the size of the supported species is limited by the probe size of the microscope (which is of the order of 1 Å), and a substantial number of supported species must be analyzed from the images to provide a statistical basis for statements about the size of the supported species.[51]

Thus, the combined use of EXAFS spectroscopy and STEM provides substantially more insight into the nuclearity and structures of the surface species than either technique alone.

The image of the sample shown in Figure 5 is among the few reported that characterize such small ensembles of a metal on a support. Samples such as supported metal clusters or ensembles must be quite stable for successful characterization by TEM. Most such samples do not yield good images, because the electron beam changes the samples, for example, causing migration and possibly sintering of the metal or because exposure to air may change the structure of the supported species.

B. Metal Clusters. Metal clusters are different from the ensembles described in the preceding section in that they have metal−metal bonds. In principle, metal clusters may be ligand-free, but in practice only gas-phase clusters may be truly ligand-free. Many supported metal clusters have been made from precursors that are metal carbonyl clusters; these may be adsorbed on supports with the metal frames intact, but the frames do not always remain intact when chemisorption of a metal carbonyl cluster occurs.

For example, $H_3Re_3(CO)_{12}$ was adsorbed on γ-Al_2O_3. The species initially formed on the support were physisorbed, without substantial changes in the cluster structure.[39,53] The metal frames in samples prepared similarly on MgO were also essentially unchanged from that of the precursor $H_3Re_3(CO)_{12}$, but on the strongly basic MgO, the precursor was deprotonated.[47]

STEM images of the physisorbed precursor clusters on γ-Al_2O_3 show the individual Re atoms, illustrating the triangular metal frame (Figure 6).[39] This is one of the few images of molecular metal clusters on a support; it required the extraordinarily high resolution offered by an aberration-corrected STEM, and the work with this sample took advantage of a capability for handling the sample and loading it into the microscope without exposure to air.[11]

Rhenium L_{III}-edge EXAFS spectra characterizing $H_3Re_3(CO)_{12}$ on γ-Al_2O_3 indicate a Re−Re coordination number of 2.1 and a Re−Re distance of 3.25 Å (and these values match, within error, those determined crystallographically for $H_3Re_3(CO)_{12}$).[53] Thus, again there is good consistency between the EXAFS and TEM results. We caution, however, that the images of Figure 6 indicate species other than $H_3Re_3(CO)_{12}$, and it is possible that the electron beam modified the sample.

When the supported rhenium carbonyl clusters were treated in H_2 at 673 K, EXAFS data showed a first-shell Re−Re coordination number of approximately 2 at an average distance of 2.67 Å, characteristic of Re−Re bonds shorter than those in bulk metallic rhenium (2.74 Å).[53] These results indicate the formation of supported rhenium clusters that are well approximated as Re_3. However, images of these clusters have not been reported. (When these supported clusters were treated at higher temperatures in H_2, the rhenium was reduced and aggregated;[54] this behavior is typical of group-7 and group-8 supported metals generally.)

Among the few examples of structurally simple and well-defined supported metal clusters characterized by both high-resolution TEM and EXAFS spectroscopy are MgO-supported osmium clusters approximated as $[Os_5C(CO)_{14}]^{2-}$. The MgO support is advantageous for measurement of high-quality TEM images of supported osmium clusters, because the low atomic weight of Mg allows a good contrast with the heavy Os atoms in bright-field, phase-contrast high-resolution TEM (HRTEM) images. Furthermore, MgO particles have been routinely found to show good stability in the electron beam. The damage of the MgO support proceeds relatively slowly, and, as a result, particles dangling over the edge of a crystallite can be imaged

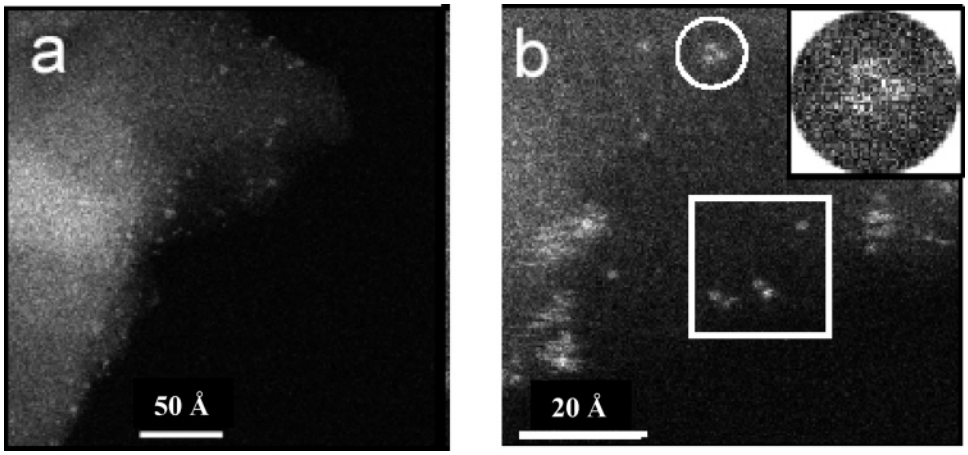

Figure 6. (a) Z-contrast STEM image of partially dehydroxylated γ-Al_2O_3-supported $H_3Re_3(CO)_{12}$; (b) higher-magnification image with a cluster circled. A cluster in side view is shown in the square.[39] From ref 39, used with permission.

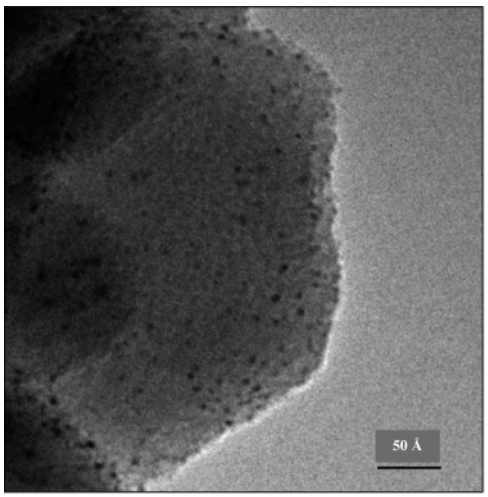

Figure 7. High-resolution TEM image of partially dehydroxylated MgO with $[Os_5C(CO)_{14}]^{2-}$ clusters dispersed on the surface (1 wt % Os).[11] Pairs of these clusters are evidently present as well as isolated clusters. From ref 11, used with permission.

with short exposure times that allow the full resolution of the TEM to be achieved.[11]

The samples were prepared by decarbonylation of initially adsorbed $Os_3(CO)_{12}$ on the partially hydroxylated surface of MgO. Treatment of the sample in CO at 548 K led to the formation of supported $[Os_5C(CO)_{14}]^{2-}$ in a high yield, together with small quantities of $H_3Os_4(CO)_{12}$ and unconverted $Os_3(CO)_{12}$. These were identified by IR spectroscopy, and $[Os_5C(CO)_{14}]^{2-}$ was also identified by extraction with a large chelating cation into a solution of acetone. ^{13}C NMR spectroscopy provided evidence of the carbido carbon atom in the pentaosmium cluster. Os L_{III}-edge EXAFS spectra characterizing the surface species indicated an Os−Os coordination number of 3.8 and an average Os−Os distance of 2.85 Å, consistent with the presence of $[Os_5C(CO)_{14}]^{2-}$.[55] However, in view of the errors, the EXAFS data are not sufficient to distinguish the predominant $[Os_5C(CO)_{14}]^{2-}$ from the other, smaller clusters present on the surface. This example illustrates how IR and ^{13}C NMR spectroscopies complement EXAFS spectroscopy for identification of the surface species.

The HRTEM image of this sample (Figure 7)[11] shows clusters of approximately 3−4 Å in diameter, consistent with the presence of osmium clusters containing no more than about five Os atoms each. Thus, the image is consistent with the spectroscopic evidence stated in the preceding paragraph. But, again, consistent with the statement above for STEM images of ensembles of osmium carbonyls on MgO, the HRTEM images alone are not sufficient to determine the cluster nuclearity because of the uncertainty in the determination of the dimensions of the metal clusters, caused in part by the Fresnel contrast effect.[52] Moreover, in TEM, image contrast is a complicated function of several parameters, including the optical properties of the equipment, the support thickness, and the cluster position and orientation on the support. Consequently, it is difficult to obtain an image that gives the best view of the structure.[52]

The osmium carbonyl clusters in this sample were decarbonylated by treatment in He at 573 K. The EXAFS data, showing a first-shell Os−Os coordination number of 3.3 at an Os−Os distance of 2.84 Å, are consistent with retention of the Os_5C moiety in the sample.[55] The TEM images bolster the EXAFS results, showing clusters of about 3−4 Å in diameter, consistent with the conclusion that the cluster frame did not break up after decarbonylation.[11] The ^{13}C NMR spectra of the decarbonylated clusters no longer provided evidence of the carbido carbon atoms, presumably because the pentaosmium clusters were bonded strongly to the support, which led to a low motional averaging of the decarbonylated clusters. Motional averaging of the large chemical shift anisotropy is necessary to observe a resonance indicative of the carbido carbon atoms. Nonetheless, these carbon atoms were inferred to be present in the decarbonylated clusters on the basis of the EXAFS evidence showing an Os−C contribution with a coordination number of 0.8 at an Os−C distance of 2.10 Å.[55]

Again, these examples illustrate the value of EXAFS spectroscopy and TEM for characterization of supported metal clusters. Used together, these techniques are much more persuasive than either alone.[56] A disadvantage of TEM arises from the fragility of the samples in the electron beam. In contrast, although the energy of the synchrotron X-ray radiation used for EXAFS experiments is high enough to excite core electrons from metals, there is a lack of evidence of structural changes of supported metals during EXAFS experiments. For example, repeated measurements of the same EXAFS functions from consecutive scans of zeolite NaY-supported gold complexes formed from $Au(CH_3)_2(acac)$ in the presence of flowing He (Figure 8) demonstrate that this sample was stable in the X-ray beam. This stability is evidently general for the samples reviewed here.

EXAFS spectra have been reported for numerous supported metal clusters, in the absence of complementary TEM images.

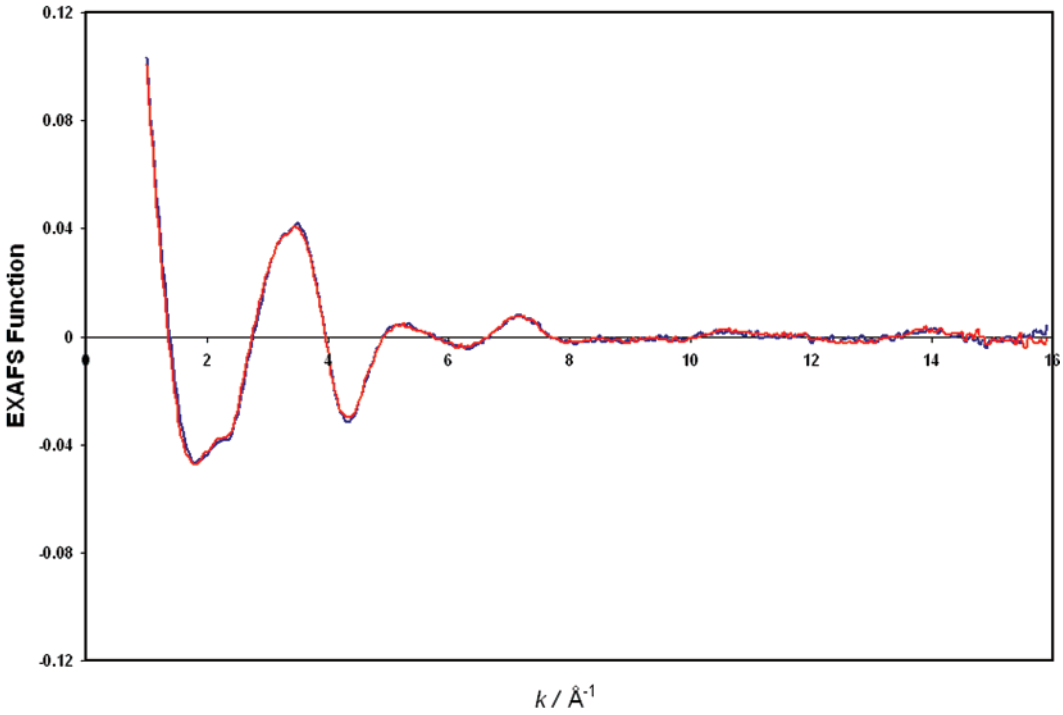

Figure 8. EXAFS functions derived from consecutive scans of a zeolite NaY-supported sample formed from $Au(CH_3)_2(acac)$ with the sample in flowing He at 298 K. The blue and the red represent separate scans.

TABLE 4: Summary of Supported Metal Clusters with Structures Determined by EXAFS Spectroscopy[a]

support	precursor	formal oxidation state of metal in precursor	method of preparation	metal−metal contribution		metal−support oxygen contribution				model of surface species	ref
						M−O_s		M−O_l			
				N	*R*, Å	*N*	*R*, Å	*N*	*R*, Å		
MgO calcined at 673 K	$Ir_4(CO)_{12}$	0	decarbonylation in He at 573 K followed by treatment with H_2 at 673 K	3.1	2.69					Ir_4	59
γ-Al_2O_3 evacuated at 298 K	$Ir(CO)_2(acac)$	1	decarbonylation in He at 573 K after flowing CO for 2 days	2.9	2.69	1.0	2.14	2.4	2.65	Ir_4	167
γ-Al_2O_3 calcined at 673 K	$Ir_4(CO)_{12}$	0	decarbonylation in He at 573 K	3.0	2.67	0.7	2.21	1.3	2.67	Ir_4	61
TiO_2 calcined at 673 K	$Ir_4(CO)_{12}$	0	decarbonylation in He at 573 K	3.1	2.68	0.9	2.05	1.5	3.21	Ir_4	63
zeolite NaY calcined at 573 K	$Ir(CO)_2(acac)$	1	decarbonylation in He at 573 K after flowing CO for 12 hours	2.9	2.66	1.2	2.15	0.7	2.63	Ir_4	62
MgO calcined at 673 K	$Ir(CO)_2(acac)$	1	decarbonylation in He at 598 K after flowing CO for 12 h at 373 K	3.8	2.64	1.3	2.08	0.6	3.33	Ir_6	77
γ-Al_2O_3 calcined at 673 K	$Rh_6(CO)_{16}$	0	decarbonylation in He at 573 K	4.2	2.67	1.1	2.07	0.7	2.89	Rh_6	72
La_2O_3 calcined at 673 K	$Rh(CO)_2(acac)$	1	decarbonylation in He at 573 K after flowing CO for 1 day	3.9	2.64	1.1	2.00			Rh_6	73
TiO_2 calcined at 673 K	$Rh(CO)_2(acac)$	1	decarbonylation in He at 573 K after flowing CO for 1 day	4.4	2.63	0.9	2.01	1.3	3.37	Rh_6	71
zeolite NaY calcined at 573 K	$Rh(CO)_2(acac)$	1	decarbonylation in He at 573 K after flowing CO for 12 h	3.9	2.68	1.1	2.17			Rh_6	70
γ-Al_2O_3 calcined at 773 K	$H_3Re_3(CO)_{12}$	1	decarbonylation in H_2 at 673 K	2.0	2.67	0.7	2.05	1.0	2.58	Re_3	53
MgO calcined at 673 K	$Os_3(CO)_{12}$	0	decarbonylation in He at 573 K after flowing CO for 4 h	3.4	2.84	1.9	1.96	1.5	3.45	Os_5C	55

[a] Notation: same as in Table 2.

The following paragraphs provide a summary and indicate the kind of information that has been obtained.

For example, $Ir_4(CO)_{12}$ and $Ir_6(CO)_{16}$ have metal frames that are tetrahedral and octahedral, respectively. Samples with these metal frames synthesized by adsorption of the above metal carbonyl clusters or by reductive carbonylation of $Ir(CO)_2(acac)$ on various metal oxides and zeolites are characterized by EXAFS spectra indicating first-shell Ir−Ir coordination numbers of approximately 3[59−63] and 4,[64−67] respectively, corresponding to the respective metal frames. When the data are of high enough quality to determine second-shell coordination numbers, second-shell Ir−Ir coordination numbers of about 1[66] have also been

determined for samples prepared by adsorption of $Ir_6(CO)_{16}$. These results are consistent with the presence of nearly uniform supported metal carbonyl clusters. Complementary evidence of the structures was obtained by IR spectroscopy[60−67] of the supported samples, showing bands that are similar to those of the crystalline $Ir_4(CO)_{12}$ and $Ir_6(CO)_{16}$ precursors, respectively; however, the matches are inexact, corresponding to the nonuniformity of environments of the adsorbed species (which leads to band broadening) and the distortion of the structures resulting from cluster-support interactions.

Indirect evidence of metal−metal bonds in supported metal carbonyl clusters is provided by ν_{CO} IR spectra; edge- and face-bridging carbonyl ligands give evidence of such bonds, for example, in two isomers of hexairidium carbonyls prepared by the reductive carbonylation of $Ir(CO)_2(acac)$ in the cages of zeolite NaY. The edge-bridging carbonyl ligands in one isomer were indicated by a ν_{CO} band at 1816 cm^{-1}, whereas the existence of a ν_{CO} band at 1730 cm^{-1} for another isomer indicated its face-bridging carbonyl ligands.[68]

Supported metal clusters with relatively well-defined structures have been prepared by decarbonylation of these and other supported iridium carbonyls, and from other metal carbonyls, including $Rh_6(CO)_{16}$. The resultant supported clusters are exemplified by Ir_4, Ir_6, and Rh_6 on metal oxides and on zeolites.[59−63,65−67,69−73] A compilation of such samples is given in Table 4, which shows EXAFS parameters characterizing a family of supported metal clusters.

The principal characterizations of these samples have been by EXAFS spectroscopy. For example, γ-Al_2O_3-supported Ir_4 clusters are characterized by an Ir−Ir coordination number of approximately 3 at an Ir−Ir distance of nearly 2.67 Å, typical of Ir−Ir bonds and consistent with the presence of tetrahedral clusters.[61] Similarly, γ-Al_2O_3-supported Ir_6[65] and γ-Al_2O_3-supported Rh_6[72] are characterized by first-shell metal−metal coordination numbers of approximately 4 (and, when the data are of high enough quality to determine second-shell coordination numbers, by second-shell coordination numbers of about 1) at metal−metal distances characteristic of chemical bonds.

An advantage of EXAFS spectroscopy is that it can be used to characterize supported catalysts as they function. (The reactivities and catalytic properties of a number of these supported clusters are reviewed elsewhere.[5,8]) For example, the structures of supported metal clusters as they were working as catalysts for ethylene hydrogenation or propylene hydrogenation have been characterized by EXAFS measurements. The results indicate the presence of Ir_4 supported on MgO[74,76] and on γ-Al_2O_3[66,74−76] and of Ir_6 and of Rh_6 on MgO.[77] These data show metal−metal coordination numbers that are consistent with the presence of tetrahedral and octahedral clusters, respectively. The EXAFS data also show that the metal−metal distances depend on both the support and the reaction environment.

In the following paragraph, we summarize limitations in the application of EXAFS spectroscopy to characterize functioning catalysts. Data can be obtained at high temperatures (e.g., catalysts in the functioning state have been investigated even at 873 K[78]). However, as the temperature increases, the thermal disorder of the sample increases. Commonly used procedures for analysis of EXAFS data are based on the assumption that the motions of the neighboring atoms around the absorbing atom are small and harmonic,[79] and this assumption is valid only for large particles and for small clusters with very low disorder (i.e., at low temperatures).[79] In the standard, widely used, EXAFS model,[30] the representation of the Debye−Waller factor implies that the disorder is small and harmonic. Therefore, the use of this model to describe samples at high temperatures leads to systematic errors, such as an apparent contraction in interatomic distances.[79] The magnitude of these errors depends on the metal and the cluster (or particle) size. For example, contractions in Pt−Pt distances in SiO_2-supported samples were found to be greater than 0.02 Å at temperatures higher than 573 K.[79] Similar results are to be expected for other supported group-8 metals. There are corrections to the standard model that attempt to account for effects of temperature on the Debye−Waller factor. These corrections are semiempirical and depend strongly on the sample.[80−82]

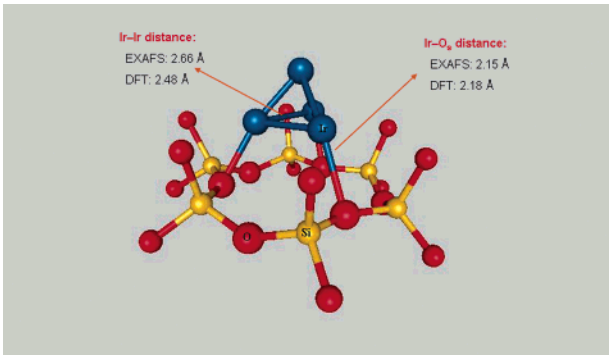

Figure 9. Structural model of Ir_4 clusters supported on a zeolite X fragment determined on the basis of EXAFS spectra and DFT calculations.[62,85] The EXAFS Ir−Ir distance is the average of the distances in the cluster. From ref 85, used with permission.

Another limitation of EXAFS spectroscopy is its inability to detect light atoms, such as hydrogen, that might be adsorbed on the metal. In most spectroscopic experiments, such small ligands are elusive, and the effect that they might have on the metal frame of the supported species is therefore difficult to determine experimentally; theory provides perhaps better opportunities than experimentation for characterizing the influence of light atoms on supported metals.

Density functional theory (DFT) has been used by numerous groups to characterize metal clusters on oxides and zeolites, and such work by the group of Rösch[83−86] includes comparisons with experimental results. They have reported calculations for bare clusters on supports and for such clusters incorporating small ligands such as CO and H.[83−87] Other calculations have been carried out to investigate small clusters on flat surfaces or in the gas phase and have been reviewed extensively.[88,89] Here we focus on theoretical results for models of supported metal complexes and clusters that account for the support and allow a direct comparison with experiment.

For example, calculations for Ir_4 supported on zeolite NaX (with the cluster assumed to be positioned at a six-ring in the zeolite) confirm the stability of the tetrahedral cluster but indicate an Ir−Ir distance 0.2 Å less than the value measured by EXAFS spectroscopy (Figure 9).[85] This difference is substantially greater than the errors expected for either DFT or EXAFS spectroscopy. DFT calculations for bare Rh_6 clusters supported on zeolite NaX indicate that the most stable bare cluster at a six-ring was a triangular twisted prism, with a twist angle of 58° (Figure 10a).[83] This value is close to that of an octahedral metal frame (as was indicated by the first-shell coordination number of nearly 4 determined by EXAFS spectroscopy[70]). However, the EXAFS spectra are not sufficient to distinguish modestly twisted prisms from octahedra; the first-shell coordination numbers determined by EXAFS spectroscopy are not sensitive to the cluster shape, and even when higher-shell information is available, the information is usually insufficient in this regard.

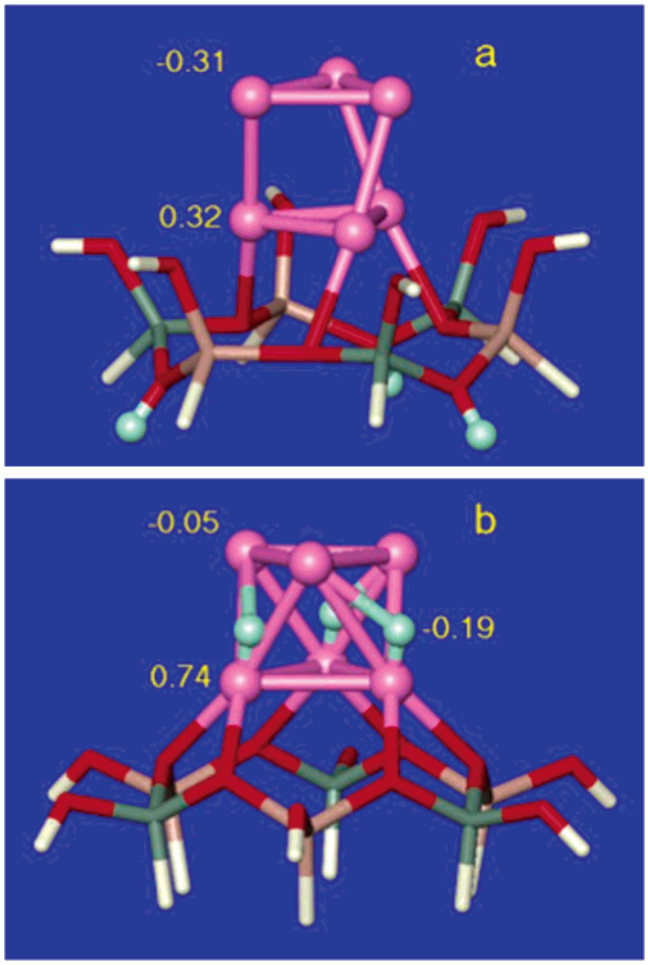

Figure 10. Structural model of Rh_6 clusters supported on a zeolite X fragment determined on the basis of EXAFS spectra and DFT calculations: (a) bare Rh_6 cluster; and (b) H-decorated Rh_6 cluster.[83] (The numbers are the calculated Mulliken charges.) From ref 83, used with permission.

As was found for Ir_4 clusters supported on zeolite X,[85] the calculated average metal−metal bond distance in the bare zeolite-supported Rh_6 clusters was found by DFT calculations[83] to be about 0.1−0.2 Å less than the EXAFS value.[70] Vayssilov et al.[83] performed calculations for the bare clusters as well as for Rh_6 clusters on the support that were decorated with hydride ligands (formed by reverse hydrogen spillover from OH groups of the zeolite). They concluded that the decorated clusters were much more stable than the bare clusters and found that the Rh−Rh distance in the decorated clusters agreed within error with the EXAFS value (Figure 10b). In a recent investigation, Vayssilov and Rösch[84] found that, quite generally, reverse spillover of hydrogen from the zeolite support onto the metal clusters is energetically favored for six-atom metal clusters (M_6) of group-8 and -11 metals. Similar results emerged from a DFT investigation of Os_5C clusters supported on MgO.[86] The calculated Os−Os bond distance[86] is about 0.3−0.5 Å shorter than the values measured by EXAFS spectroscopy,[55] indicating that the Os_5C clusters were not ligand free (Figure 11).

These results suggest that the cleaning of surfaces of supported metals required for the successful measurement of metal dispersions with hydrogen chemisorption measurements[83] may not always be possible, because temperatures high enough to clean the metal surface by evacuation could lead to restructuring of the metal, such as changes in the morphologies of the supported species or sintering of the metal on the support surface.

All of these calculations at the density functional level to characterize supported metal clusters complement the results from EXAFS spectroscopy, which is not sensitive enough to provide a good basis for assessing the presence of small ligands decorating the metals. These ligands evidently influence significantly the structures of the metal frames of supported metals. Although the cluster nuclearity may remain unchanged upon addition of ligands, changes in the metal frame could result in changes in many of the properties of supported metals that affect their reactivities. These results show the value of theory in complementing experiment to assess such issues.

So far, we have considered the application of TEM and EXAFS and IR spectroscopies and theoretical calculations in the elucidation of nuclearity of supported metal clusters and ensembles. Other techniques, including Raman, far-IR, and UV−visible spectroscopies, can provide valuable complementary information, but the available data are fragmentary for the class of materials considered here. A brief summary of the use of these other techniques to investigate the nuclearity of supported metal clusters follows.

Raman spectroscopy is valuable for characterization of metal clusters, because it can be used to measure a wide range of vibrational frequencies and it is particularly useful for low-frequency vibrations (those below 1000 cm^{-1}, and sometimes as low as 50 cm^{-1}), which pertain to metal−metal bonds. Although IR spectroscopy can be used to detect bands with frequencies as low as approximately 10 cm^{-1}, absorption by the cell window material (e.g., KBr) typically cuts off bands at low frequencies (e.g., roughly 450 cm^{-1} for KBr). Therefore, Raman spectroscopy is potentially more useful than IR spectroscopy to detect low-frequency vibrations that characterize metal−metal bonds in metal clusters.

In several experiments, low-frequency spectra were recorded that give evidence of metal−metal vibrations of supported carbonyl clusters of osmium and of iridium. In the triosmium carbonyl clusters bonded to γ-Al_2O_3 that were formed from $Os_3(CO)_{12}$, Deeba et al.[90] detected a strong band at 160 cm^{-1} and a broad band with maxima at approximately 80 and 119 cm^{-1}. Considering the symmetry reduction of the sample compared with the precursor, Knözinger[91] assigned these bands to three Os−Os stretching modes. In an investigation of $Ir_4(CO)_{12}$-derived clusters supported on MgO and containing 6 wt % Ir, Mestl et al.[92] detected bands at 121, 165, and 212 cm^{-1}, attributed to vibrations of the Ir_4 frame; a clear assignment of the bands to specific modes could not be made. The authors were unable to obtain high-quality spectra of samples containing only 1 wt % Ir. Thus, the Raman data provide evidence of metal carbonyl clusters on supports, but they are less than incisive indicators of the cluster structures.

Highly dispersed metal clusters consisting only of a few metal atoms resemble molecular clusters, for which numerous solution Raman spectra have been reported. The uniformity of the clusters discussed in this review should lead to sharp, distinctive bands. Thus, some researchers have been led to the conclusion that Raman spectra of decarbonylated clusters on support should in principle be measurable; however, recent attempts have not been successful.

There are several reasons for the lack of Raman spectra of decarbonylated metal clusters on supports:[15−18] (1) The heating effect of the laser beam might cause the reduction and sintering of the supported metal clusters. This effect becomes more severe when the samples are colored, which is true for most supported metal cluster samples. (2) Raman spectroscopy usually has low sensitivity associated with the inherently low Raman scattering

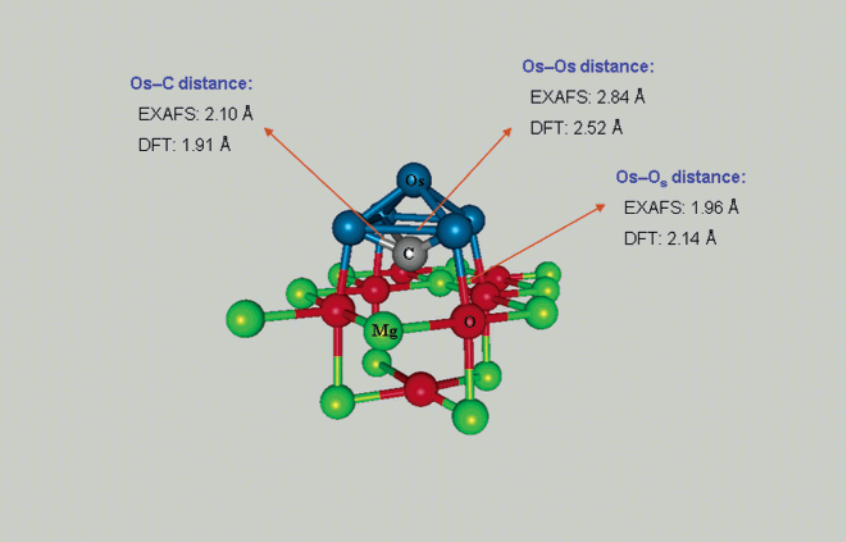

Figure 11. Structural model of Os_5C clusters supported on partially dehydroxylated MgO at a defect site determined on the basis of EXAFS spectra and DFT calculations.[55,86] The EXAFS Os−Os distance is the average of these distances in the cluster. The apical Os−C distance determined by DFT is 2.62 Å. From ref 86, used with permission.

cross-sections. When the metal loadings are low in supported catalysts (these values are typically about 1−3 wt %), the signals may be too weak to detect. (3) Background fluorescence can overwhelm the Raman spectrum. This fluorescence can be caused by surface impurities or by surface hydroxyl groups. An efficient method for reducing background fluorescence is to use a lower excitation frequency. However, this is done at the expense of signal intensity. (4) Although Raman spectroscopy can be used to characterize samples under high-temperature reaction conditions, blackbody radiation at high temperatures (>1000 K, for example) can cause severe background effects. (5) It is difficult to obtain quantitative information from Raman spectroscopy, as the scattering cross sections of the supported surface species usually remain unknown.

In principle, far-IR spectroscopy could also be used to detect metal−metal vibrations in supported metal clusters. However, lattice vibrations of the supports are strong in the same region (wavenumbers less than 1000 cm^{-1}) in which metal−metal vibrations are expected. Therefore, there is a lack of examples of the use of this technique to determine nuclearity of supported metal species.

Many samples of supported metal clusters are colored, and UV−visible spectra show absorption bands that are related to the separation of the metal frontier orbitals.[19] Typically, spectra are recorded in the diffuse reflectance mode, because scattering losses are too severe in the transmission mode.[19,93]

Supported osmium clusters have been characterized by UV−visible spectroscopy.[94] Samples were prepared by chemisorption of $Os_3(CO)_{12}$ on SiO_2. UV−visible spectra characterizing the samples after evacuation showed the presence of bands at 309, 360, and 410 nm. The first two bands were assigned to the electronic transitions within the molecular orbital structure of the triangular framework. Similar absorptions[95] (at 330 and 385 nm) were observed for the precursor $Os_3(CO)_{12}$.

4. Oxidation States of Metals in Supported Metal Complexes and Clusters (XANES, EXAFS, and IR Spectroscopies; TPR/TPO; DFT)

In organometallic chemistry, one uses the formalism of simple oxidation states such as 0, +1, +2, etc, to assign a charge to a metal, realizing that it is an approximation.[96,97] Typically, electron counting rules[96,97] are applied to account for the degree of coordinative saturation of metals in organometallic compounds. Many coordinatively unsaturated metal complexes are important in homogeneous catalysis.

The electron counting rules of organometallic chemistry have been applied to provide evidence of formal oxidation states of metals in surface complexes. A major complication in electron counting pertaining to supported metal complexes arises from the fact that the bonding between the metal and the support is not necessarily known, and even when experimental methods and theoretical calculations provide a description of this bonding, questions remain about how to count the number of electrons offered by the support as a ligand.[98]

Therefore, structural information from EXAFS and IR spectroscopies characterizing ligands in a supported metal complex (providing a basis for application of electron-counting rules) is not sufficient to estimate with confidence the oxidation state(s) of metals. Furthermore, when the samples contain metal clusters, electron-counting rules are more difficult to apply, because knowledge of the exact bonding of each metal atom in the supported cluster is required.

Thus, information from complementary techniques is needed, and electron counting has been of limited value in the context of the subject of this review. The next paragraphs include a brief evaluation of the experimental methods, and examples of their application follow.

TPR and TPO, whereby samples are treated in flowing H_2 or O_2, respectively, as the sample temperature is ramped, allow estimation of the oxidation state(s) of supported metal species. In these experiments, the H_2 or O_2 uptakes are measured and correlated with the stoichiometric quantities required to reduce or oxidize a standard sample, respectively. Thus, TPR and TPO provide quantitative information characterizing the oxidation state(s) of a supported metal.

XANES spectra can also be used to estimate oxidation state(s) of supported metals. Typically, one compares the XANES of the supported metal species with XANES of a reference compound (usually in crystalline form), for which the formal oxidation state of the metal is known. However, the comparison is not always straightforward, as the XANES signature is sensitive to the ligand environment of a metal in a complex, and to the size, structure, and ligand environment of metals in clusters. Thus, XANES provides only qualitative information

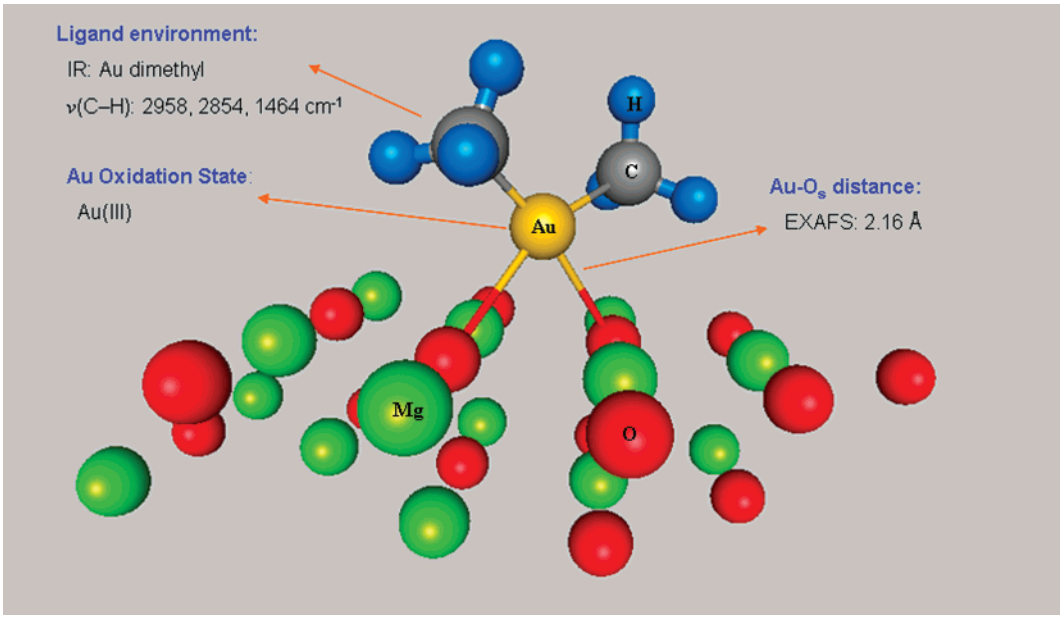

Figure 12. Structural model of mononuclear gold complex bonded to partially dehydroxylated MgO determined on the basis of IR and EXAFS spectra as well as XANES and TPR and TPD.[99,100]

and should be used in concert with TPR and TPO to provide the most incisive information.

X-ray photoelectron and Mössbauer spectroscopies are also useful to estimate oxidation state(s) of supported metals, but the use of these techniques to investigate the types of samples discussed in this review has been limited.

Theoretical calculations complement the aforementioned characterization methods by predicting the stability of supported metals in a given oxidation state. The combination of theoretical and experimental methods provides the most insight into the estimation of metal oxidation states when the samples are structurally simple and uniform, such as those reviewed here.

Metals on supports are commonly present in cationic complexes, with support oxygen atoms or OH groups being ligands bonded to the metal. In many catalysts, metals are present on supports as zerovalent clusters or particles, although recent results, mentioned below, indicate that the metal atoms at the metal−support interface are cationic.[83] There is also evidence indicating that metals in some small clusters on oxide supports may be entirely cationic. Details of samples illustrating these points and the methods of determining the metal oxidation states follow.

A. Mononuclear Metal Complexes. An example of the characterization of a supported metal complex by temperature-programmed methods is provided by MgO-supported gold complexes prepared by the reaction of $Au^{III}(CH_3)_2(acac)$ with partially hydroxylated MgO.[99] When the supported complexes, $Au^{III}(CH_3)_2\{OMg\}_2$ (where the braces denote groups that are part of the support surface; Figure 12), identified by IR and EXAFS spectroscopies,[100] were reduced in flowing H_2 as the temperature was ramped from 300 to 673 K, the H_2 uptake was found to be 1.51 ± 0.15 molecules of H_2 per Au atom, consistent with the reduction of Au^{III} to metallic gold. In the reverse process, metallic gold clusters were oxidized to Au^{III} as the temperature was ramped from 300 to 800 K with the sample in flowing O_2.[99]

In this case, the methods provided incisive information, because the sample initially contained gold complexes in a unique oxidation state (+3). However, TPR and TPO are not always sufficient, because the H_2 and O_2 uptakes may not always be ascribed exclusively to single redox processes. For example, a metal might be present in various oxidation states, or the support might incorporate species that could be oxidized or reduced (such as cations on the support surface or adsorbed carbonates, which are formed from exposure of basic supports such as MgO and La_2O_3 to CO_2 of the atmosphere). Then, complementary data from other techniques are needed.

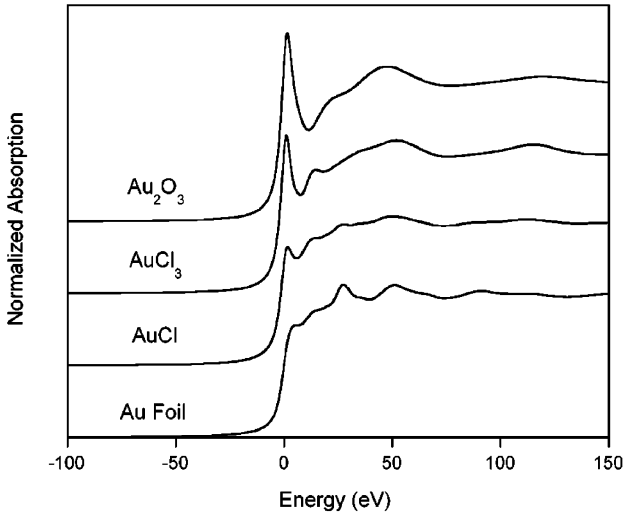

Figure 13. XANES spectra at the Au L_{III} edge characterizing various gold reference compounds.[101] From ref 101, used with permission.

XANES data, which are essentially qualitative, nicely complement the quantitative TPR and TPO data. To be most informative, XANES spectra should be obtained under transient conditions matching those of the TPR and TPO experiments (as the temperature is ramped and the sample is treated in H_2 or O_2, respectively). For example, Au L_{III}-edge XANES was used to characterize the supported gold complexes mentioned above.[99] XANES may allow one to distinguish between Au^0, Au^I, and Au^{III} on the basis of the distinct features (Figure 13) they exhibit in the spectra,[101] and so XANES in combination with quantitative TPR and TPO results then may allow a characterization accounting for all of the oxidation states of supported gold. However, interpretation of XANES is not always straightforward. For example, if a mixture of Au^0 and Au^{III} is present, the spectra could resemble that of Au^I.

The results show XANES features characteristic of Au^{III} for the initially prepared sample, as evidenced by the following features in the spectra, which are characteristic of Au^{III} complexes both in the crystalline state and on supports: (a) the position of the absorption edge at 11923 eV, (b) the presence of a prominent feature centered at an energy 4 eV higher than the absorption edge (white line), and (c) the presence of shoulders at 15 and 50 eV higher than the X-ray absorption edge.[99] The spectrum included features at 15 and 25 eV higher than the absorption edge, and the absorption edge shifted to 11919 eV, which is characteristic of Au^0 (and observed for gold foil), when the temperature reached 480 K as the sample was treated in flowing H_2. This temperature matches that at which the H_2 uptake in the TPR experiments indicated the reduction of Au^{III} to Au^0. Thus, the qualitative information provided by XANES complements quantitative information provided by temperature-programmed methods.

EXAFS data showing bonding of the metal complex to the support bolster the XANES and TPR/TPO results showing evidence of Au^{III} complexes in the initially prepared sample. EXAFS spectra indicate an Au−O distance of 2.16 Å (Figure 12), which is characteristic of a bond between a gold cation and oxygen of the support. Similar metal−oxygen distances are found in other cationic group-8 metal complexes bonded to supports.[40,46,47,69]

An advantage of XANES spectroscopy is that it can be used to characterize supported metal catalysts in reactive atmospheres. For example, XANES spectra recorded at steady state as the MgO-supported gold complexes described above catalyzed the hydrogenation of ethylene[102] show features characteristic of Au^{III}, consistent with EXAFS spectra showing the lack of aggregation of the gold under the same conditions. These results indicate that supported mononuclear Au^{III} complexes are catalytically active for alkene hydrogenation in the absence of zerovalent gold. Similarly, Au^{III} complexes bonded to the surface of high-area La_2O_3 were found to be highly active CO oxidation catalysts,[103] and XANES spectra provided evidence of the lack of reduction of the Au^{III} during catalysis.

In contrast, the oxidation states of rhodium on supports are not easily distinguished by XANES. Rhodium may be present in the 0, +1, and +3 oxidation states, but Rh K-edge XANES spectra are too complex to discriminate them and sometimes do not even indicate which ones are present.The complexity in the spectra is related to the fact that the XANES of a specific metal atom depends not only on the oxidation state of the metal in the complex but also strongly on the geometry and nature of the ligands.[104] Therefore, the use of reference compounds to estimate oxidation states of supported rhodium is limited, because the choice of appropriate reference compounds remains a challenge. Developments in the theory of XANES might help to interpret spectra and resolve the effects of structure and oxidation state of the metal on the XANES signal.

In the absence of insight from XANES spectra to estimate the oxidation state of supported rhodium, the use of IR spectroscopy or other techniques that provide information about the ligands bonded to the metal is beneficial. For example, some evidence of the oxidation state of the rhodium in $Rh(CO)_2$ complexes bonded to zeolite Y (which had been calcined at 573 K), discussed in section 3, emerged from ν_{CO} spectra (Figure 1) showing bands at 2116 and 2050 cm^{-1}. These bands are similar to bands observed in ν_{CO} spectra of numerous dicarbonyls of Rh^I.[40] Thus, the IR data point to the conclusion that the formal oxidation state of rhodium in the supported complexes was +1.

Theoretical calculations at the density functional level confirmed the conclusion, forming part of the basis for the structural model shown in Figure 2.[40] The Mulliken charge of the Rh was estimated to be +0.53 e, which is consistent with the presence of Rh^I.

B. Ensembles of Mononuclear Metal Complexes. As illustrated above, mononuclear metal complexes can be prepared in groups (or ensembles) on support surfaces, most efficiently by reaction of molecular precursors containing more than one metal atom. Characterization of surface ensembles involves the methods stated above and others that pertain to supported metal complexes generally; determination of the oxidation states of the metals in surface ensembles requires the above-stated methods used to estimate oxidation states of metals in supported complexes.

The aforementioned samples made from $H_3Re_3(CO)_{12}$ on MgO were characterized by IR spectra that are consistent with the initial formation of the deprotonated rhenium clusters $[H_2Re_3(CO)_{12}]^-\{MgO\}$.[47] Subsequent treatment led to breaking of the Re−Re bonds and formation of ensembles of mononuclear rhenium carbonyl complexes, inferred to be present in ensembles of several Re atoms. EXAFS data characterizing the supported complexes show a Re−O distance of 2.15 Å, consistent with cationic rhenium bonded to oxygen of the support.

C. Metal Clusters. Samples made from $H_3Re_3(CO)_{12}$ on γ-Al_2O_3 (after decarbonylation) were characterized by an EXAFS first-shell Re−Re coordination number of approximately 2, indicating the formation of three-atom units, and these were regarded not as ensembles of rhenium complexes but instead as clusters represented as Re_3, as explained above.[53] The Re−Re distance estimated from EXAFS spectra of the supported clusters is 2.67 Å. This distance is characteristic of the metal−metal bonds in cationic clusters of rhenium.[105] There are several examples of molecular trinuclear clusters of niobium and tantalum in solution that have similar metal−metal distances.[106−108] In these samples, the metal atoms in the clusters are cationic and stabilized by the presence of ligands. Thus, the EXAFS results characterizing the supported clusters indicate that the rhenium atoms in them are cationic.

EXAFS spectra give further indirect evidence of cationic rhenium, as evidenced by the presence of bonds between the rhenium and O atoms of the support at an average Re−O distance of 2.05 Å, which is a typical distance characterizing bonds between rhenium cations and oxygen atoms. The supported Re_3 structures are inferred to be raft-like, consisting of three Re atoms bonded to each other in a triangular fashion and coordinated to O atoms of the support. Thus, this example shows that the support is a ligand for the rhenium clusters, as explained below. All the Re atoms are inferred to be cationic.

These results are bolstered by Re L_{III}-edge XANES spectra characterizing the supported Re_3 and showing features that are consistent with the presence cationic rhenium, with oxidation states between approximately +4 and +6.[53]

The above example illustrates the value of the combined application of XANES and EXAFS spectroscopies to the characterization of metal oxidation states in supported metal clusters. These methods can also be used to track changes of metal oxidation states in samples under reaction conditions, as illustrated by the following example.

Supported gold nanoparticles (with nonuniform structures) have drawn wide attention recently because highly dispersed supported gold is an active catalyst for numerous reactions, including CO oxidation.[109] Supported gold nanoparticles of

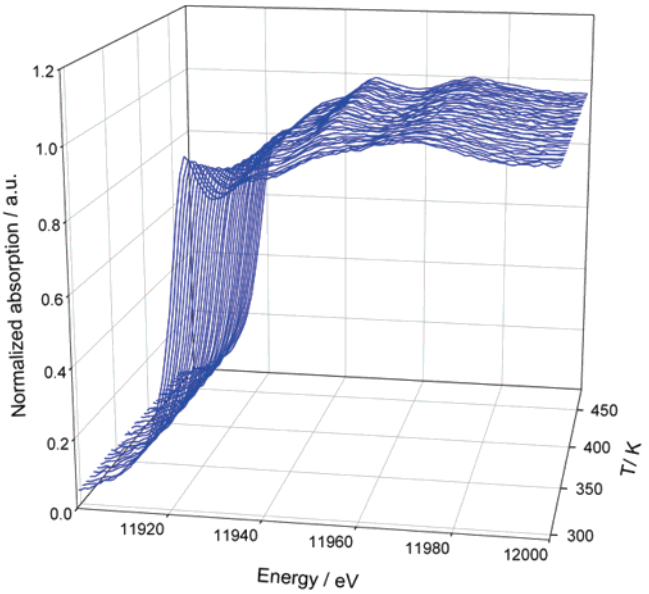

Figure 14. Time-resolved XANES spectra characterizing the formation of TiO_2-supported gold nanoparticles from the supported mononuclear gold complex made by bringing $Au(CH_3)(acac)$ in contact with partially dehydroxylated TiO_2. The sample was treated in flowing He (760 Torr) at increasing temperature.[111] From ref 111, used with permission.

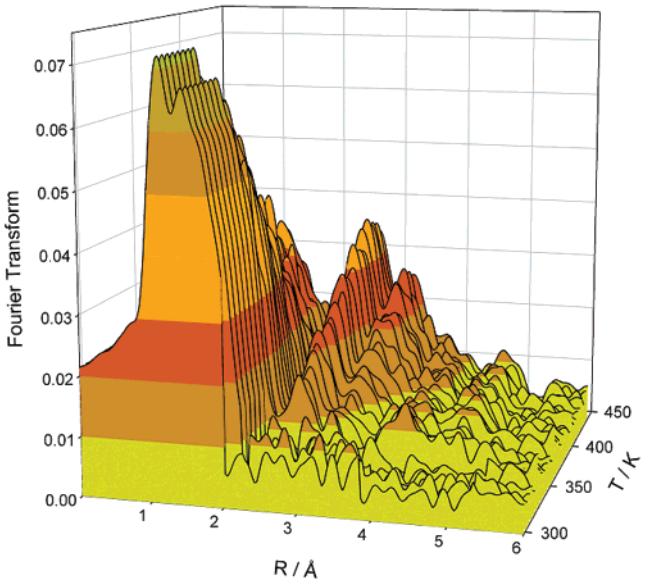

Figure 15. Fourier transform (k^0-weighted, uncorrected) of time-resolved EXAFS spectra characterizing the formation of TiO_2-supported gold nanoparticles from the supported mononuclear gold complex made by bringing $Au(CH_3)(acac)$ in contact with partially dehydroxylated TiO_2. The sample was treated in flowing He (760 Torr) as the temperature was increased.[111] From ref 111, used with permission.

various average sizes on MgO,[99] γ-Al_2O_3,[110] and TiO_2[111] have been prepared from initially adsorbed $Au^{III}(CH_3)_2(acac)$ by gentle sintering of the metal originally present in the form of mononuclear Au^{III} complexes bonded to approximately 2 oxygen atoms of the support, as exemplified by the structural model in Figure 12.

Time-resolved XANES spectra were recorded to follow the formation of TiO_2-supported gold nanoparticles from initially present TiO_2-supported Au^{III} complexes (Figure 14). With modern synchrotrons, a time-resolved XANES spectrum can be collected in less than about one minute, allowing fine-grained monitoring in real time of the changes in oxidation state of a metal.[111] The time resolution of the spectra allowed the determination of the temperature at which the Au^{III} was reduced to Au^0 on the support.[111] Furthermore, EXAFS spectra recorded simultaneously with the XANES (with a spectrum recorded approximately every 2 min), show that the onset of reduction of the gold corresponds almost exactly to the onset of aggregation to give supported gold clusters (Figure 15).[111] These results demonstrate that reduction and aggregation of supported gold occur simultaneously and show how time-resolved EXAFS spectra (when measured in concert with time-resolved XANES) help provide understanding about the oxidation state of a supported metal.

However, we caution that the XANES spectra show features that are consistent with the presence of mixtures of both cationic (either Au^{III} or Au^{I}) and zerovalent gold in the early stages of reduction of Au^{III}. The mixtures complicate the assignment of the oxidation states of the gold in the sample.

Although attempts have been made to conduct semiquantitative analyses of XANES spectra to determine the relative amounts of a metal in particular oxidation states,[112,113] the fact that the ligand environment and the size(s) of the metal clusters also affect the XANES signal complicates matters.[114] Therefore, one should use the qualitative information obtained from XANES in concert with quantitative information provided by techniques such as temperature-programmed methods to determine the relative amounts of a supported metal present in various oxidation states.

So far, we have discussed examples for which XANES spectra in combination with TPR, TPO, and EXAFS spectroscopy provide information about the oxidation state(s) of a metal in a supported cluster. In some cases, all the metal atoms are inferred to be cationic, and in others, mixtures of zerovalent metal and metal cations have been inferred to be present. The question arises about how these might coexist in the same supported clusters.

Theoretical results characterizing Rh_6 in a faujasite zeolite indicate that some metal atoms in clusters on a zeolite support are positively charged and that the positive charge of the cluster is borne almost entirely by the metal atoms at the metal−support interface (Figure 10).[83] The metal atoms farther from the interface are essentially uncharged. The theoretical result is consistent with the EXAFS results mentioned above and the conclusion that supported group-8 metal clusters are bonded to the supports by metal−oxygen bonds with distances of about 2.1−2.2 Å[84,85] (the value calculated for Rh_6 on the zeolite was 2.2 Å). The Mulliken charge of each Rh atom at the metal−support interface in Rh_6 on the zeolite was estimated to be 0.76 e. This value compares with the Mulliken charge of 0.53 e of the rhodium atom in $Rh(CO)_2$ bonded to zeolite DAY (Figure 2);[40] the results are consistent with the suggestion that the Rh atoms at the interfaces in each sample should be represented formally as Rh^I.

These results can be generalized to other supported metal clusters, exemplified by the γ-Al_2O_3-supported Re_3 clusters discussed above, which were inferred to have a raft-like structure, in which each Re atom was bonded to O atoms of the support.[53]

Mössbauer spectroscopy is another technique that provides information about the oxidation state(s) of metals, even in reactive atmospheres.[119] Iron, tin, iridium, ruthenium, platinum, and gold are among the supported metals that have been investigated with this technique. However, there is a lack of examples of the characterization of samples that are as simple and uniform structurally as the ones discussed in this review.

X-ray photoelectron spectroscopy (XPS) is another technique that provides information about the oxidation state(s) of

supported metals, but similar to Mössbauer spectroscopy, it has not been used to characterize samples such as those considered here. Until recently, there had been a lack of XP spectra of samples in the presence of reactive atmospheres, but, by using synchrotron radiation, researchers have recently been able to report good XPS results measured at pressures up to 5 mbar.[120,121]

Extensive reviews of Mössbauer spectroscopy[119,122] and XPS[123−125] are available.

5. Characterization of Ligands on Supported Metals (IR, NMR, and EXAFS Spectroscopies; DFT)

By the term "ligand" we refer to any group bonded to a metal atom or cluster. The ligands include the support itself, but in this section we focus on ligands that are not part of the support (support ligands are considered in the following section about metal−support interactions). Generally, two classes of ligands can be distinguished: those present after synthesis of the supported species from the precursor compound and those formed by subsequent treatment of the supported species.

The former ligands may include some present in the precursor compound, which raises the question of how the precursors are chosen. So far, there is no one general strategy for this choice. The principal requirement for purposes of preparing nearly uniform molecular analogues on supports is that adsorption of the precursor should give uniform metal species bonded to the support and isolated from each other; high catalytic activity and selectivity of the resultant surface species are also common goals of the synthesis.

Many metal complexes and a large fraction of the known molecular metal clusters incorporate ligands including the elements P, N, S, or As, such as phosphines, amines, etc. Although many of these ligands stabilize metal cluster frames (even when the clusters are adsorbed), they are typically resistant to dissociation from the metal (or the support), complicating characterization of the supported metal-containing species and typically inhibiting catalysis.

Thus, the ligands in the molecular precursors of choice usually do not include elements other than C, H, and O. This constraint severely narrows the list of appropriate metal cluster compounds, and almost all the available candidates are metal carbonyls (many with no ligands other than carbonyls).

There are several reasons why metal carbonyl clusters are good precursors of uniform supported metal clusters: (1) CO is a good electron-donor ligand that stabilizes metal cluster frames and is small enough to allow coordinative saturation of these frames, hence stabilization of the compound. CO represents a good compromise, as the stabilization of the cluster frame is counterbalanced by the loss of catalytic activity caused by CO acting as a reaction inhibitor (because it bonds strongly to the metal in competition with reactants). (2) Decarbonylation of supported clusters without breakup of the metal frame or sintering of the metal is sometimes possible under relatively mild conditions (section 3B), making it possible to obtain supported clusters from which the CO ligands have been completely removed. (3) CO is a reactive ligand that is an intermediate in some catalytic reactions (such as CO oxidation) and therefore presents a head start for some catalysis experiments (such as conversion of CO bonded to a metal by reaction with O_2). (4) CO is a widely used probe molecule that is especially useful for characterization of metal species by IR spectroscopy. Valuable information about the symmetry, the metal oxidation state, and other ligands bonded to a metal center can be obtained from the spectra in the ν_{CO} region. Furthermore, other techniques provide evidence of CO as a ligand, including ^{13}C NMR spectroscopy, EXAFS spectroscopy, and TPDE, which can be used straightforwardly with the adsorbed precursor.

A major class of precursor for supported metal complexes is organometallic compounds with ligands restricted to the elements C, H, and O. Hydrocarbons are particularly attractive ligands, offering numerous choices ranging from small methyl groups to bulky neopentyl groups, which protect the highly reactive M−C bond by steric hindrance. Many hydrocarbons (exemplified by alkyls) bond to metals at the carbon atom and are thus distinct from organic ligands that bond to the metal via oxygen atoms (such as acac, a commonly used ligand in metal complexes used as precursors of supported catalysts). Metal−carbon bonds are highly reactive, and hydrocarbon ligands can often be removed from supported metal complexes under mild conditions, with the metal species left unagglomerated. (In contrast, metal carbonyl clusters typically remain (largely) intact during adsorption on the support.) Precursors incorporating organic ligands may readily undergo significant structural changes when they are adsorbed on a support, for example, by the elimination of a ligand and its replacement by the support (such as reaction of a methyl ligand with a support hydroxyl group to give methane and a metal−surface oxygen bond).

An important issue in the choice of ligands is how well they can be identified. Because of the structural complexity of some organic ligands, their characterization may be more difficult than characterization of carbonyls, for example. Suitable techniques for the structural characterization of organic ligands include NMR and IR spectroscopies.

A. Characterization of CO Ligands. Metal carbonyls are the most widely used class of precursors for the synthesis of nearly uniform supported metal clusters, and they are commonly used for the preparation of supported mononuclear metal complexes as well. The resultant supported metal species usually retain CO ligands from the precursor, and these provide valuable structural information in the vibrational spectra in the ν_{CO} region. The CO vibrations can be recorded by several techniques, including IR and Raman spectroscopies, with the former being a simple, widely applied method that exhibits excellent sensitivity. What makes the spectroscopy of the CO vibration particularly appealing is the relative straightforwardness of the interpretation of the signals of the CO species. The measured frequency is sensitive to the nature of the metal−CO bond and is therefore characteristic of the metal to which the CO is bonded; furthermore, the spectra distinguish CO that is terminally bonded to the metal and CO that bridges two (or three) metal atoms. The ν_{CO} spectra also provide evidence of the symmetry of the metal complex and thus information about ligands other than CO bonded to the metal (including the support).

Among the best-characterized metal complexes on supports are rhodium carbonyls, including the $Rh(CO)_2$, described above. These Rh^I species are formed from precursors such as $Rh(CO)_2$(acac);[40] from $Rh(allyl)_3$, followed by treatment of the surface species in CO;[126] from aqueous solutions of salts such as $[Rh(NH_3)_5Cl][OH]_2$, followed by treatment of the surface species in CO;[127] or by oxidative fragmentation of supported rhodium clusters.[128] Rhodium carbonyls were among the first supported metal complexes to be investigated in depth, because the intense ν_{CO} bands in the IR spectra provide so much structural information. Transmission IR spectra recorded in the ν_{CO} region characterizing $Rh(CO)_2$ on zeolites are shown in Figure 1. IR spectra characterizing samples at frequencies below 1000 cm^{-1}

are typically unobservable because of the absorption by the support. As a result, the detection of δ_{CO} modes is hindered.

^{13}C NMR spectroscopy is also useful for characterization of supported metal carbonyls, illustrated by the characterization of carbonyl ligands in a sample containing a mixture of $Rh_6(CO)_{16}$ and $[Rh(CO)_2]^+$ on zeolite NaY.[129] The shielding parameters characterizing the dicarbonyls in $Rh_6(CO)_{16}$ and $[Rh(CO)_2]^+$ were not distinguishable, but the two species could be resolved and their amounts quantified because of a large difference in T_1 relaxation. This result complements the IR spectra in which the two carbonyl species were resolved (but could not be accurately quantified).[129]

EXAFS spectroscopy provides complementary information about supported metal carbonyls. When a supported metal cluster has both terminal and bridging CO ligands, the EXAFS errors are relatively large, in part because only average information is obtained. Thus, deconvolution of the metal−carbon and metal−oxygen shells characterizing metal carbonyls in EXAFS spectra cannot be done with confidence.

In contrast, when the species have only terminal CO ligands, as in $Rh(CO)_2$, then metal-edge EXAFS data provide valuable complementary information about the metal−ligand moieties, giving evidence of both the metal−carbon and metal−oxygen contributions, including the metal−carbon and metal−oxygen coordination numbers and distances, as well as evidence of the interactions between the metal and oxygen atoms of the support (discussed below). The multiple scattering in the nearly linear metal−C−O moieties is helpful in identification of these structures.

For example, in the determination of the structure shown in Figure 2, EXAFS data representing $Rh(CO)_2$ in dealuminated Y zeolite demonstrated the presence of approximately 2 CO ligands per Rh atom, as the Rh−C coordination number was found to be 2.2 and the Rh−O coordination number 2.3, consistent with the IR evidence of the symmetry.[40] The long metal−oxygen distance (3.03 Å) provided further confirming information of the existence of the carbonyl ligands.

In summary, the structure of $Rh(CO)_2$ is shown by IR, ^{13}C NMR, and EXAFS spectra and confirmed by calculations at the density functional level; the Rh atom is well approximated as Rh^I. Further discussion below (section 6A) is concerned with how and where the complex is bonded to the support.

Other thoroughly characterized oxide-supported metal carbonyl complexes include $Re(CO)_3$ on porous MgO powder; such complexes were synthesized from $HRe(CO)_5$, $DRe(CO)_5$, $Re_2(CO)_{10}$, and $H_3Re_3(CO)_{12}$.[47,130] Complementary spectroscopic techniques and temperature-programmed-decomposition and -reduction data demonstrated the presence of three CO groups per Re atom.

For example, MgO-supported $Re(CO)_3$ prepared from $H_3Re_3(CO)_{12}$ was characterized by IR, inelastic electron tunneling, and EXAFS spectroscopies. Three ν_{CO} bands were observed in the IR spectrum, at 2028, 1905, and 1862 cm^{-1}. Similarly, three ν_{CO} bands were detected in the inelastic electron tunneling spectrum (2045, 1920, and 1825 cm^{-1}).[131] Moreover, additional information, obscured in the IR spectrum by support absorbances, was observed in the low-wavenumber region of the tunneling spectrum. A doublet at 410 and 468 cm^{-1} was assigned to Re−C stretching vibrations on the basis of reported Raman, IR, and tunneling spectra.[131]

Consistent with these results, EXAFS characterization of this sample showed a Re−C contribution at 1.88 Å with a coordination number of 3, and a Re−O contribution at 3.09 Å with a coordination number also of 3.[47] All the results indicate the formation of rhenium tricarbonyls on the support.

IR spectra in the ν_{CO} region also characterize the reductive carbonylation of supported $[Ir(CO)_2]^+$ species, leading to the formation of CO-coordinated Ir_4 clusters, $Ir_4(CO)_{12}$. The process was followed by IR spectroscopy to characterize the clusters on both calcined and uncalcined zeolite NaY.[132] When the zeolite had been calcined at 573 K, the IR spectra included ν_{CO} bonds that grew in and then disappeared, indicating the appearance of an intermediate thought to be $Ir_2(CO)_8$, as there were ν_{CO} bands observed at 2096, 2053, 2039, and 1818 cm^{-1} that essentially match those of $Ir_2(CO)_8$. In contrast, the IR spectra characterizing the sample supported on uncalcined zeolite NaY included no evidence of such intermediates. Because similar spectra were obtained for the two samples at the end of the process, it was inferred that $Ir_4(CO)_{12}$ formed on both supports. A band pattern characteristic of $Ir_4(CO)_{12}$ was also observed for species on other supports, such as γ-Al_2O_3 and TiO_2. In contrast, when the supports were the more strongly basic MgO and zeolite NaX, the formation of $[HIr_4(CO)_{11}]^-$ was observed.[60,133]

Supported metal carbonyls can also be characterized efficiently by TPDE. A major advantage of TPDE is that it can provide quantitative information. Identification of the gases evolved helps to elucidate the transformation of the surface species, especially when the results are combined with spectroscopic characterization of the surface species.[35,36]

B. Organic Ligands. Many supported metal complexes have organic ligands such as hydrocarbons, typically alkyls. Suitable techniques for characterization of organic ligands in these species are IR and ^1H and ^{13}C NMR spectroscopies.

Characterization of supported organometallic species by NMR spectroscopy may be challenging because of the low overall density of organic species in the typical sample. However, recent progress in NMR spectroscopy has made possible the determination of organic ligands in supported metal complexes with a precision comparable to that attainable routinely for molecular compounds. For example, Petroff et al.[134] showed that two-dimensional (2D) heteronuclear correlation (HETCOR) solid-state NMR spectroscopy with MAS can be used in the same way as in experiments characterizing solutions.

Several recent examples illustrate the determination of structures of organic ligands on oxide-supported metal complexes by solid-state high-resolution 2D NMR spectroscopy. The use of ^1H-^{13}C 2D HETCOR made possible verification of the attribution of the various signals obtained by one-dimensional (1D) NMR spectroscopy, as shown, for example, in work reported by the group of Basset et al.[134−137] They synthesized supported complexes of group-4 to group-7 metals by adsorption of $[M(tBu)_4]$ (with M = Ti, Zr, Hf), $[M(=CHtBu)(CH_2tBu)_3]$ (with M = Ta), $[M(\equiv CtBu)(CH_2tBu)_3]$ (with M = Mo), or $[M(\equiv CtBu)(=CHtBu)(CH_2tBu)_2]$ (with M = Re) on partially dehydroxylated SiO_2 that had been treated at temperatures between 773 and 973 K. The surface species (Figure 16) were characterized by IR and 1D and 2D NMR techniques.

Early ^{13}C-MAS NMR spectroscopic investigations of **1** (Figure 16) showed that only the intense signal of the methyl species (observed at 33.9 ppm for the complex of Zr) could be detected, whereas the carbon atoms of the methylene groups bonded to the metal as well as of the quaternary carbon atoms of the neopentyl groups could not be observed.[138] The former is related to a long relaxation time T_1 for CH_2. The peak corresponding to the quaternary C atoms, which is expected at ca. 30 ppm, could not be observed because of the line

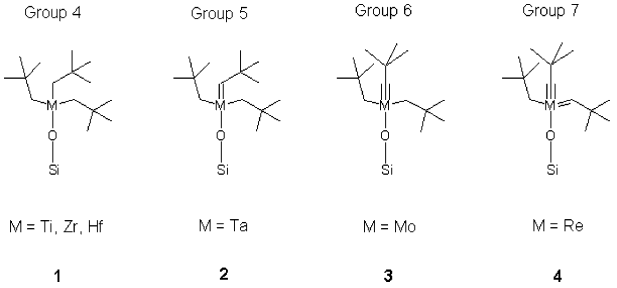

Figure 16. Complexes of group 4 to group 7 metals bonded to partially dehydroxylated silica.

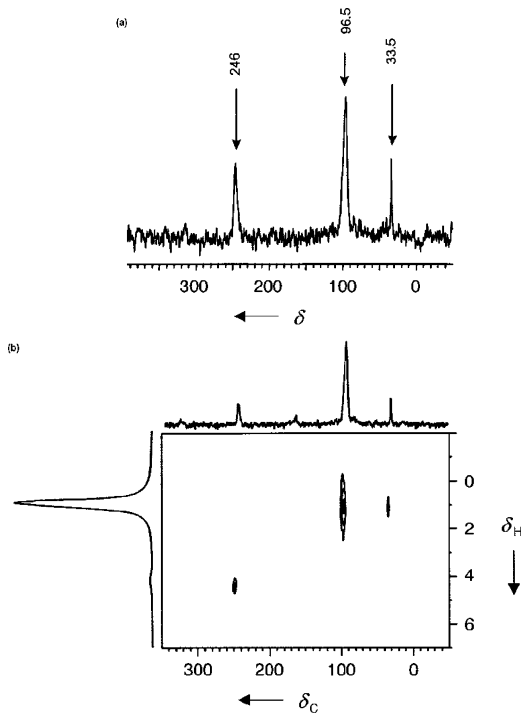

Figure 17. (a) Solid-state CP MAS ^{13}C NMR spectrum of tetrakis-(neopentyl) neopentylidene tantalum bonded to partially dehydroxylated silica; (b) 2D HETCOR NMR spectrum of tetrakis(neopentyl) neopentylidene tantalum bonded to partially dehydroxylated silica.[135] From ref 135, used with permission.

broadening in the solid-state spectra. In general, in all of the surface metal alkyls, the carbon atoms in the alpha position are especially important, because their identification shows how the organic ligands are bonded to the metal. However, these are the most difficult to detect.

Species **2** (Figure 16) was characterized by high-resolution solid-state 1D and 2D NMR spectroscopy.[135] The ^1H NMR spectrum of **2** includes a resonance at 4.2 and a broad resonance at 1.0 ppm. The solid-state cross polarization (CP) MAS ^{13}C NMR spectrum of **2** that had been partially ^{13}C-enriched in the alpha position led to a spectrum showing three resonances, at 246, 96.5, and 33.5 ppm (Figure 17a). These were unequivocally assigned by 2D HETCOR NMR spectra showing a correlation between the signals at 4.2 ppm (^1H) and 246 ppm (^{13}C) as well as the two signals at 33.5 and 96.5 ppm (^{13}C) and the broad resonance at 1 ppm (^1H) (Figure 17b). The former correlation is attributed to the carbene carbon and the proton attached to it, and the latter strongly suggests that the broad resonance at 1 ppm is related to the methylene and methyl protons.

Detection of the ^{13}C signal of the carbynes in **3** and **4** (Figure 16) has been challenging because the intensity cannot be enhanced by the cross polarization technique as a consequence of the lack of hydrogen atoms in the alpha or beta positions. In addition to ^{13}C enrichment and the conventional cross polarization (CP) technique, HP-DEC (high-power decoupling) NMR spectroscopy has been shown to be valuable for increasing the intensities of weak signals. Carbon atoms in various positions were detected in **3** and **4** with this technique.[134,139]

Although solid-state NMR spectroscopy is a powerful technique for the determination of the organic ligands in supported metal complexes, the difficulty of spinning of samples in reactive atmospheres limits the application of MAS NMR spectroscopy (section 2). IR spectroscopy, on the other hand, is well suited to the characterization of ligands on metal complexes in reactive atmospheres, as illustrated by the following examples.

Uniform tetrahedral metal clusters consisting of nearly four Ir atoms supported on MgO or on γ-Al_2O_3, described above, are catalytically active for the hydrogenation of ethylene and of propylene.[66,75,76] EXAFS spectra recorded during catalysis gave evidence of isolated Ir_4 clusters on the supports.[66,75] For each catalyst, organic ligands were observed on the clusters by IR spectroscopy, with the identifications being based upon comparisons with the spectra of reference compounds incorporating these ligands or upon the spectra of these groups on metal surfaces. The organic species that were inferred to be present on the γ-Al_2O_3-supported Ir_4 clusters under conditions of catalytic ethylene hydrogenation (with $P_{C_2H_4} > 200$ Torr) include ethyl (2956, 2933 cm^{-1}), π-bonded ethylene (3060, 3026 cm^{-1}), di-sigma-bonded ethylene (2988, 2975, 2897, 2884 cm^{-1}), and ethylidene (2947, 2896 cm^{-1}), which were distinguished on the basis of their ν_{CH} vibrational modes.[66]

When propylene reacted in the absence of H_2 with Ir_4/Al_2O_3, IR and ^{13}C NMR spectra indicated the formation of propylidene bound to the cluster ($CH_3CH_2CIr_4$).[75] In the presence of H_2, however, cluster-bound dehydrogenated propylene (approximated as C_xH_y, such as, for example, C_3H_2, or C_2H) as well as propylidyne was observed.

C. Hydride Ligands. Supported transition metal hydrides are of interest because of their involvement in catalytic reactions such as alkane metathesis and hydrogenolysis,[140−144] among others. The principal characterization techniques used for the hydride ligands include ^1H NMR and IR spectroscopy. Inelastic neutron scattering spectroscopy is also suited for the characterization of hydride ligands.

As mentioned in the preceding section, the reaction of tris-(neopentyl) neopentylidene tantalum with partially dehydroxylated SiO_2 led to the formation of surface organotantalum complexes. The SiO_2-supported tantalum(III) monohydride species $\{\equiv SiO_2\}Ta^{III}H$ has been suggested to form as a result of treatment of these complexes under 1 atm of H_2 at temperatures up to 473 K. Characterization of the hydride ligands in this complex was done by IR spectroscopy.[145]

When the surface organotantalum complexes were heated to 473 K in H_2, the IR bands in the range of 2700−3000 cm^{-1} (ν_{CH}) and 1300−3000 cm^{-1} (δ_{CH}), corresponding to the neopentyl or neopentylidene groups, progressively decreased in intensity. Simultaneously, a set of new bands appeared in the region near 1800 cm^{-1}, which are assigned to ν_{TaH} vibration modes. This assignment was confirmed by IR spectra characterizing the H/D exchange.[145]

Although IR spectroscopy can be used to detect hydride ligands, it is usually not sensitive enough to distinguish hydrides in various coordination environments. For example, the reaction of $\{SiO\}Zr(CH_2tBu)_3$ with H_2 at 423 K led to the formation of two different zirconium hydrides: $\{SiO\}ZrH$ and $\{SiO\}ZrH_2$. When these were characterized by IR spectroscopy, one peak

was observed in the region in which zirconium hydrides would be expected, 1600−1650 cm^{-1}. The peak (at 1638 cm^{-1}) was assigned to ν_{ZrH}.[146]

The zirconium hydrides were further characterized by ^1H NMR spectroscopy. The spectrum included signals at 0.8, 4.4, 10.1, and 12.1 ppm. The two downfield signals at 10.1 and 12.1 ppm can be assigned to two types of zirconium hydride species. Moreover, these two signals show distinct T_1 values, consistent with the presence of two kinds of hydrides in different environments. To further identify these two hydride species, a more advanced ^1H NMR technique, double-quantum (DQ) proton spectroscopy with MAS, was applied. Two-dimensional multiple-quantum (MQ) proton spectroscopy, including double-quantum and triple-quantum proton spectroscopy, is a powerful technique to probe the structure and dynamics associated with proton−proton dipolar coupling. The strong autocorrelation peak observed for the proton resonance at 12.1 ppm indicates a close proximity between the two protons involved in this correlation. Therefore, it was assigned to $\{\equiv SiO\}ZrH_2$. In contrast, a proton resonance at 10.1 ppm was assigned to the surface species $\{SiO\}ZrH$, which shows only a weak correlation. This weak correlation likely arises from the interaction between $\{SiO\}$-ZrH and protons of $\{SiO\}ZrH_2$.[146]

Hydride ligands have also been detected on supported metal clusters. As mentioned in section 3B, DFT calculations indicate that zeolite X-supported Rh_6 clusters do not exist as bare clusters. Instead, the hexarhodium clusters with bridging hydride ligands are much more stable.[83,84] Unfortunately, no experimental characterizations have been done for this sample to test the calculated results. However, other zeolite-supported metal clusters, zeolite Y-supported Ir_6, were investigated by ^1H NMR and inelastic neutron scattering vibrational spectroscopies.[147] The results give evidence of hydride ligands, even with the sample in the absence of gas-phase H_2.

La_2O_3-supported Rh_6 clusters were used to catalyze ethylene hydrogenation, and IR spectra recorded during the reaction indicated the presence of hydride ligands. The intensities of the vibrational modes at 2020 and 1940 cm^{-1} were observed to increase from zero at the start of the reaction in a flow reactor to maximum values during steady-state catalysis. The assignment of these two signals to Rh−H stretching was confirmed by isotope exchange experiments.[73]

So far, we have presented examples of the use of various spectroscopic techniques that illustrate the determination of structures of organic and hydride ligands on zeolite- and metal oxide-supported complexes and clusters. Beyond this, gas-phase analyses by gas chromatography (GC) and mass spectrometry (MS) of ligands formed from the supported species (e.g., in temperature-programmed desorption experiments) can complement the spectroscopic information obtained by NMR, IR, EXAFS, and the other techniques discussed above.

The characterization of tris(neopentyl) neopentylidene tantalum **2** on the partially dehydroxylated surface of SiO_2 provides a good example. It was found that the gaseous product of the reaction of $Ta[CH_2C(CH_3)_3]_3[=CHC(CH_3)_3]$ with partially dehydroxylated SiO_2 was neopentane, as identified by GC/MS.[148,149] Simultaneously, the surface silanol bands decreased in intensity, and the ν_{CH} and δ_{CH} bands increased in intensity, suggesting the formation of chemisorbed organotantalum species **2** (Figure 16). The reaction was also carried out with deuterated SiO_2. In this case, mass spectrometry indicated a mixture of nondeuterated and deuterated neopentane. The presence of some deuterated neopentane demonstrates that at least some of the neopentane was formed as a result of reaction between tantalum and the surface silanol groups.[148]

6. Metal-Support Interactions (EXAFS, IR, and Raman Spectroscopies; DFT)

Stabilization of the dispersion of the supported species described here is strongly associated with the metal−support interactions that may hinder the migration and possible reduction and coalescence of the metals on the supports. Thus, the supports not only provide high-area platforms for anchoring of the metal species, they also can be considered to be ligands to the metal. Therefore, understanding of the metal−support interactions requires insight into the bonding between the metal atoms of the supported species and surface atoms of the support.

In this review, we focus on examples for which the metal−support interactions can be described in terms of chemical bonds and ignore the more complex interactions that are sometimes classified under the name of "strong metal−support interactions" and may involve migration of the support onto the metal species.

Most of the characterization of metal−support interfaces has emerged from EXAFS spectroscopy, from which metal−oxygen contributions have been identified and inferred to characterize bonding of supported metals to oxygen atoms of the supports. EXAFS spectroscopy has been successful in the characterization of metal−support interfaces of the samples discussed in this review, because the supported metal species in these samples are small, which maximizes the fraction of metal atoms that are in contact with the support.[150] Because EXAFS spectroscopy provides only average information about the local structure surrounding the supported metal, the technique is more incisive in the characterization of the metal−support bonding of supported mononuclear metal complexes than in the characterization of supported metal clusters, because all the metal atoms are bonded to the support in the former and not necessarily in the latter.

The degree of uniformity of both the support and the metal species influences the detail in which the metal−support interface can be described. The surfaces of the metal oxides used as supports in the samples described here are nonuniform, exposing various sites and defects for bonding of the metal species. In contrast, zeolites are crystalline, providing, in prospect, opportunities to anchor metal species at nearly equivalent sites. Because some zeolite-supported metal species are more nearly uniform and better defined structurally than the analogous oxide-supported species, the zeolite-supported samples provide the best available opportunities of understanding of the metal−support interface.

A. Metal−Support Interactions in Mononuclear Metal Complexes. Some of the most incisive structural information about metal−support interfaces has emerged from EXAFS characterization combined with quantum-chemical calculations of supported metal complexes. An example is provided by the aforementioned rhodium carbonyls bonded to a zeolite.[40]

EXAFS data characterizing $Rh(CO)_2$ bonded to zeolite Y are summarized in Table 2. EXAFS spectra indicated three plausible structural models of the supported complex. Although all three models accounted for two carbonyl ligands bonded to the Rh atom, they differed in the Rh−support interactions. In model I, the Rh atom was bonded to three oxygen atoms of the support, at a distance of 2.09 Å, whereas in models II and III each Rh atom was bonded to two oxygen atoms, with different Rh−O distances (2.15 and 2.09 Å for models II and III, respectively).[40]

Because the structure of the supported complex could not be determined fully by the experimental results, quantum-chemical

calculations were used to resolve the ambiguity. DFT calculations indicated that each Rh atom was bonded to two oxygen atoms at a distance of 2.20 Å, similar to the results found for the Rh−O contribution in model II. The calculation also identified a nearby Al center at a distance of approximately 2.80 Å from the Rh atom, comparable to the experimental Rh−Al distance of 2.73 Å found for model II.[40] Furthermore, calculations provided evidence of the location of the rhodium dicarbonyl complexes, showing that the most favored structure on the surface corresponds to the $Rh(CO)_2$ complexes bonded at a four-ring of the zeolite-framework (Figure 2). The supported complexes were inferred to be nearly uniform on the basis of the sharpness of the ν_{CO} bands in the IR spectra, as shown in Figure 1; thus, it was inferred that most of the complexes were bonded to crystallographically equivalent sites on the zeolite support (Figure 2).[40]

The above example shows how spectroscopic characterization and calculation can be used in combination to determine the structure and location of a supported metal complex. Another example showing the value of combining spectroscopic and theoretical characterization is a MgO-supported rhenium tricarbonyl complex. The results show how the pretreatment of the support affects the metal−support interactions. As mentioned in section 5A, MgO-supported $Re(CO)_3$ can be prepared from various rhenium carbonyl precursors. For example, it was prepared from $Re_2(CO)_{10}$ on samples of MgO that had been pretreated under vacuum at temperatures in the range 673−973 K.[151] The various pretreatments of the MgO support changed its degree of hydroxylation and affected the interactions between rhenium atoms and the support surface.

IR spectra indicated the symmetry and two limiting-case structures, present on dehydroxylated MgO (calcined at 973 K) and on hydroxylated MgO (treated with a stream of helium saturated with water), respectively.[151] On the largely dehydroxylated MgO, three ligands in the structures, other than the carbonyl ligands, were inferred to be oxygen (O^{2-}) ligands of the support (the surface species was $Re(CO)_3\{OMg\}_3$). In contrast, the three other ligands on the hydroxylated MgO powder were OH ligands of the support (in $Re(CO)_3\{HOMg\}_3$).[151] A partially hydroxylated MgO (with approximately 1.9 times as many surface OH groups as oxygen ions) was inferred to contain predominantly $Re(CO)_3\{HOMg\}_2\{OMg\}$.[151] The identification of the ligands in these species was based on ν_{CO} and ν_{OH} spectra of the samples and comparison with those of molecular analogues.

The interaction between the rhenium tricarbonyl and the MgO support was also characterized by Raman spectroscopy for a sample prepared from the precursor $H_3Re_3(CO)_{12}$.[131] The spectrum includes two broad peaks, at 800 and 1050 cm^{-1}. That at 800 cm^{-1} is inferred to represent a Mg−O−Re vibration, and that at 1050 cm^{-1} is assigned tentatively to a Re−(O(H)−Mg) mode. EXAFS data are consistent with the IR and Raman spectra and indicate the presence of approximately 3 support oxygen atoms per Re atom in the surface structures (Table 2).[47]

The structural model of $Re(CO)_3\{OMg\}_3$ was further characterized by DFT calculations.[50] The structure parameters calculated for $Re(CO)_3\{OMg\}_3$ bonded at a corner cation defect site of MgO are in good agreement with the experimental results. The Re−O_s distance determined by EXAFS spectroscopy (2.15 ± 0.03 Å) agrees well with the theoretical value of 2.15 Å (Figure 4). The theoretical results show that the Re−O bond energy in $Re(CO)_3\{OMg\}_3$ (3.5 eV) is greater than the Re−CO bond energy (2.4−2.5 eV), confirming the role of the oxide support as a strongly bonded ligand, in this case tridentate.

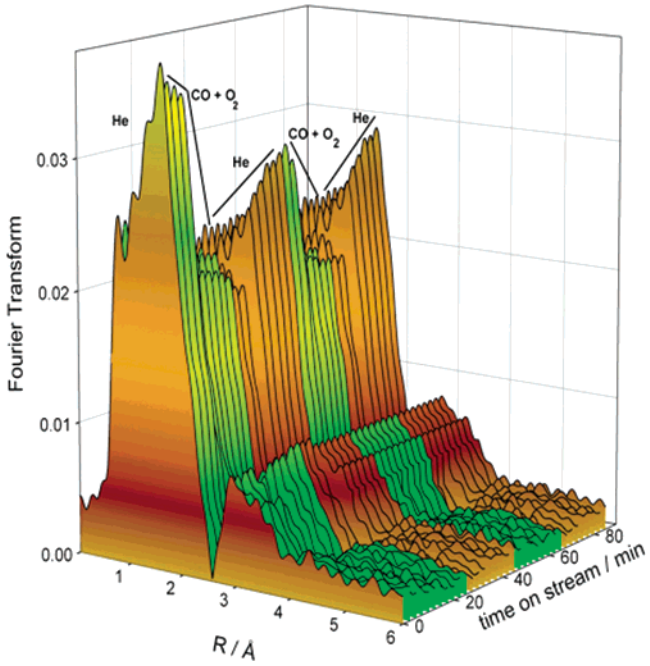

Figure 18. Fourier transform (k^0-weighted, uncorrected) of time-resolved EXAFS spectra characterizing the changes in the metal−support interface as mononuclear gold complexes in zeolite NaY functioned as CO oxidation catalyst at 298 K and 760 Torr.[154] From ref 154, used with permission.

The results characterizing these and other surface metal complexes lead to the following generalizations: The metal−oxygen distances in metal oxide-supported complexes of group 7 and group 8 metals are 2.1 ± 0.1 Å,[150] and these distances are essentially the same as the metal−oxygen distances determined by X-ray diffraction crystallography for complexes of the same metals containing electron donor oxygen ligands, including $[Ru(CO)_2(OCOCF_3)(\mu\text{-}OSiMe_2CH_2PPh_2)]_2$[152] and $[Re(CO)_3(\mu_3\text{−}OH)]_4$.[153] Thus, metal oxides and zeolites are electron-donor ligands to the supported metal complexes.

Metal−support interactions may change during catalytic reactions, depending on the reaction conditions and the strength of the metal−oxygen bonds. EXAFS spectroscopy is one of the techniques that allow monitoring of changes in the metal−support interface as supported metals are exposed to reactive atmospheres.

Time-resolved EXAFS spectra were recorded to follow changes in the metal−support interface as mononuclear gold complexes in zeolite NaY functioned as CO oxidation catalysts at 298 K.[154] As the gold remained mononuclear, initial contact with CO and O_2 led to the rapid formation of gold complexes bonded (on average) to two O atoms of the zeolite, as evidenced by an Au−O contribution with a coordination number of approximately 2 at a distance of 2.16 Å (Figure 18). Further contact with the reactive mixture led to breaking of one Au−O bond to give mononuclear gold complexes bonded (on average) to approximately one O atom of the support, as evidenced by the decrease in the Au−O coordination number from approximately 2 to approximately 1. At the same time, the Au−O distance increased to 2.24 Å. These changes were reversed in the absence of the reactive mixture, indicating that two supported mononuclear gold complexes interchanged as a result of the switch of flowing gases. These results are the first evidence of changes in a metal−support interface in real time during a catalytic reaction.

B. Metal−Support Interactions in Supported Metal Clusters. Characterization of metal−support interactions in supported

TABLE 5: Strengths and Limitations of Characterization Methods to Determine Structures of Supported Metal Complexes and Clusters

method	strength(s)	limitation(s)
EXAFS spectroscopy	information about nuclearity of supported species, even in reactive atmospheres; information about metal−ligand, (including metal−support) interactions	provides only average information; limited to low temperatures; hydrogen atoms bonded to metal atoms cannot be identified; light backscatter atoms (such as C, O, and N), cannot be distinguished from each other
TEM	information about size and location of supported species	no images of isolated supported metal complexes have been reported; little work reported for samples under reactive atmospheres; electron beam may damage samples; little work reported with aberration-corrected microscopy
XANES spectroscopy	information about oxidation state(s) of supported metals, even in reactive atmospheres	provides only average, qualitative information; depends on geometry, size, and ligand environment of metal species; need for use of appropriate references to interpret spectra
XPS	information about oxidation state(s) of supported metals (even in reactive atmospheres at low pressures)	depends on size of metal species and ligand environment; usually requires UHV conditions; charging effects significant, depending on support
TPR/TPO	quantitative information about oxidation state(s) of supported metals	redox reactions may involve species other than the supported metal
IR spectroscopy	information about ligands on metal; information about oxidation state(s) of metal (e.g., when CO is used as a probe molecule)	assignment of bands may not be straightforward; use of CO as a probe molecule could change structure of supported species
Raman spectroscopy	information about geometry of metal species; information about metal−metal bonds in metal clusters; information about metal−ligand interactions; can be used with samples in reactive atmospheres	weak signals as a consequence of low sensitivity of technique; heating effects of beam could change structure of supported species; background fluorescence could prevent measurement of spectra representing sample
UV−visible spectroscopy	information about metal−metal bonds in metal clusters	information may not be specific enough to allow identification of surface species
density functional theory	can account for metal, ligands, and (model of) support	representation of support is usually simplified

metal clusters by EXAFS spectroscopy is more complex than characterization of such interactions in supported metal complexes. In supported metal clusters, the metal atoms are usually not in equivalent positions on the surface. Only the atoms at the metal−support interface form chemical bonds with the support oxygen atoms. As EXAFS spectroscopy provides only average information, it is not sufficient by itself to characterize fully the metal−support interactions. However, for small clusters, EXAFS results can give some insights into the sample structure, especially when used in combination with other characterization techniques and quantum-chemical calculations.

EXAFS results characterizing metal−oxygen (M−O) contributions in oxide- and zeolite-supported metal clusters (Table 4) indicate distances in the range of 2.1−2.2 Å.[150] Other metal−oxygen contributions are typically found at distances of about 2.5−2.7 Å. The shorter metal−oxygen ($M-O_s$) distances are bonding distances, essentially matching those in supported metal complexes and distances determined by X-ray diffraction in molecular metal complexes in which metal ions are bonded to oxygen, as mentioned in section 6A. The longer metal−oxygen distances ($M-O_l$) of about 2.6 Å suggest weak interactions between the metal and surface oxygen atoms; these interactions are not well understood.

The EXAFS results have been confirmed by quantum-chemical calculations. DFT calculations for Ir_4 clusters in zeolite X (assumed to be present at a six-ring, Figure 9) indicated Ir−O distances of about 2.18 Å, in good agreement with the range of $M-O_s$ distances from EXAFS data. A $M-O_l$ contribution at 2.66 Å was also found by calculation.[85] Similarly, theoretical results representing Os_5C on MgO (Figure 11) indicate $Os-O_s$ distances of about 2.1 Å, in good agreement with the EXAFS data.[86]

Quantum-chemical calculations can also help to identify the specific sites of the support where the metal clusters are bonded. It has been suggested on the basis of theoretical calculations[155−157] and scanning tunneling microscopy images of clusters on flat surfaces[58] that defects on metal oxides may serve as sites to anchor the metal clusters. However, the representation of the support in theoretical calculations is usually limited, as described above, and the flat surfaces for which images are available lack the structural complexity of typical supports, which also contain hydroxyl groups and water on their surfaces.

To illustrate the possible role of defect sites on supports on the stabilization of metal clusters, calculations were carried out for Os_5C on MgO (Figure 11); bonding on the stable square (001) face as well as at cation defect sites was considered. The results indicate that Os_5C is bonded markedly more strongly at these surface defect sites than at defect-free sites (Figure 11). The binding interaction of Os_5C on the MgO(001) surface at cation defect sites (V_s centers) is 4.84 eV greater than the value characterizing the cluster bonded at a defect-free site on the same surface.[86] The results seem likely to be general; metal clusters on metal oxides are expected to be present predominantly at defect sites. (This generalization may extend to mononuclear metal complexes on metal oxides as well.)

7. Summary and Opportunities

Mononuclear metal complexes and clusters of a few atoms each anchored to high-area metal oxides and zeolites have been synthesized precisely to be structurally simple and nearly uniform. They have been characterized in depth by the application of complementary experimental and theoretical techniques, yielding structural models represented in terms of the nuclearity of the metal species, the formal oxidation state(s) of the metal, and the ligands (including the support) bonded to the metal. Some of the properties of these samples, such as the metal−support-oxygen bond distances and the stabilization of the supported clusters by decoration with hydride ligands, are suggested to extend to the complex structures typical of supported metal catalysts used in industry.[83]

Because no single physical technique is sufficient in the characterization of such samples, it is generally desirable to use as many of the appropriate techniques as possible (Table 5).

The techniques providing the most insight into the structure and bonding of supported metal species include X-ray absorption, NMR, and vibrational spectroscopies; transmission electron microscopy; and density functional theory. Fundamental understanding of the structure and bonding of a supported metal complex or cluster demonstrates how the individual structural properties are related to each other. For example, the degree of aggregation of a metal on a support gives an indication of its principal oxidation state; understanding of how ligands bond to a metal may help to elucidate the metal nuclearity and oxidation state; and understanding of the bonding between a metal and atoms of the support may provide evidence of the oxidation state of the metal atoms at the metal−support interface.

We believe that further investigation of precisely synthesized supported metal complexes and clusters will provide fundamental understanding to pave the way to materials with new properties and to new insights into the nature of more complex materials such as industrial catalysts. Investigation of well-defined supported metal species with the physical methods reviewed here is also expected to stimulate development of these methods.

Acknowledgment. We thank the following people for help, collaboration, and insightful comments over the course of many years: L. F. Allard, J.-M. Basset, N. Browning, K. Hadjiivanov, J. F. Haw, Y. Iwasawa, H. Knözinger, D. C. Koningsberger, J. J. Rehr, and N. Rösch. We thank our colleagues V. A. Bhirud, J. Guzman, and S. Nemana for help in preparation of the manuscript. This work was supported by the U.S. Department of Energy, Office of Energy Research, Office of Basic Energy Sciences, Division of Chemical Sciences, contract FG02-87ER13790 (Y.H., B.C.G.) and the National Science Foundation, grant number CTS-0121619 (J.C.F.-G.) and a Feodor Lynen Fellowship awarded by the Alexander von Humboldt Foundation to S.K.

Appendix: X-ray Absorption Spectroscopy

XAS (i.e., EXAFS and XANES spectroscopies) requires a continuous and tunable source of high-intensity X-rays (normally a synchrotron). A double-crystal monochromator is used to select the X-ray energy range. Absorption of the X-ray beam by the sample depends on the beam energy. The X-ray absorption spectrum generally exhibits a smooth decreasing intensity with increasing energy, except at an absorption edge, where the absorption coefficient increases abruptly. This happens when the photon energy is high enough to excite an electron from a core level of the atom.[30] Samples such as those considered here are investigated at the metal K- and/or L-edges (Table 1).

After the core electron is excited, it can be transferred to a vacant excited state or to the continuum, depending on the photon energy. If it has enough energy to be transferred to the continuum, it is scattered by neighboring atoms. The scattering process is indicated in the absorption spectrum as the fluctuations in the absorption coefficient.[30]

The XANES region of the absorption spectrum extends to about 30 to 50 eV beyond the absorption edge. It provides information about the local electronic environment of the absorbing atom, which serves as a basis for estimation of the metal oxidation state(s).[31,32] The EXAFS region includes oscillations of the X-ray absorption coefficient that may extend to energies about 1000 eV higher than the absorption edge. This region is dominated by single-scattering events, in which the outgoing electron is scattered only once by the atoms neighboring the absorber atom.[33] The oscillatory part of the absorption coefficient in the EXAFS region contains the structural information that can be used to characterize the surroundings of the absorber atoms.

The first step in the analysis of EXAFS spectra is to isolate the EXAFS from the total absorption data. This is done by removal of the smooth absorption of the isolated absorber atom (background removal). One method for removal the background consists of fitting the total absorption coefficient with polynomial splines using a least-squares procedure.[30] The resultant spline is a smooth function that is then removed from the total absorption to isolate the EXAFS.

Usually, the resulting EXAFS function is presented in *k*-space (*k* is the photoelectron wave-vector, which is proportional to the difference between the incoming photon energy and the binding energy). The oscillations in the EXAFS function are related to interatomic distances between the absorber (metal) atom and the nearby scattering atoms as well as the number of neighboring atoms (coordination number) and their identities. The information is readily observable as a result of a Fourier transformation of the *k*-space data. Sayers et al.[34] showed that Fourier transformation of the EXAFS function results in a radial distribution function (in *R*-space). The contributions of various shells in the X-ray absorption spectrum may be identified in the *R*-space plots.

References and Notes

(1) Walzer, J. F., Jr. *U.S. Patent* 5,643,847, 1997.
(2) McVicker, G. B.; Kao, J. L.; Ziemiak, J. J.; Gates, W. E.; Robbins, J. L.; Treacy, M. M. J.; Rice, S. B.; Vanderspurt, T. H.; Cross, V. R.; Ghosh, A. K. *J. Catal.* **1993**, *139*, 48.
(3) Jentoft, R. E.; Tsapatsis, M.; Davis, M. E.; Gates, B. C. *J. Catal.* **1998**, *179*, 565.
(4) Dossi, C.; Fusi, A.; Psaro, R.; Roberto, D.; Ugo, R. *Mater. Chem. Phys.* **1991**, *19*, 191.
(5) Gates, B. C. *Chem. Rev.* **1995**, *95*, 511.
(6) Ugo, R.; Dossi, C.; Psaro, R. *J. Mol. Catal. A* **1996**, *107*, 13.
(7) Copéret, C.; Chabanas, M.; Petroff Saint-Arroman, R.; Basset, J.-M. *Angew. Chem., Int. Ed.* **2003**, *42*, 156.
(8) Guzman, J.; Gates, B. C. *Dalton Trans.* **2003**, 3303.
(9) Bäumer, M.; Freund, H.-J. *Prog. Surf. Sci.* **1999**, *61*, 127.
(10) Freund, H.-J.; Bäumer, M.; Kuhlenbeck, H. *Adv. Catal.* **2000**, *45*, 333.
(11) Allard, L. F.; Panjabi, G. A.; Salvi, S. N.; Gates, B. C. *Nano Lett.* **2002**, *2*, 381.
(12) Peri, J. B. In *Catalysis−Science and Technology*; Anderson, J. R., Boudart, M., Eds; Springer-Verlag: Heidelberg, 1984; Vol. 5, p 176.
(13) Howe, R. F. In *In Situ Spectroscopy in Heterogeneous Catalysis*; Haw, J. F., Ed; Wiley-VCH: Weinheim, 2002; pp 140−143.
(14) Komiyama, M.; Obi, Y. *Rev. Sci. Instrum.* **1996**, *67*, 1590.
(15) Stair, P. C. In *In Situ Spectroscopy in Heterogeneous Catalysis*; Haw, J. F., Ed; Wiley-VCH: Weinheim, 2002; pp 125−129.
(16) Knözinger, H. *Catal. Today* **1996**, *32*, 71.
(17) Knözinger, H.; Mestl, G. *Top. Catal.* **1999**, *8*, 45.
(18) Mestl, G. *J. Mol. Catal. A* **2000**, *158*, 45.
(19) Knözinger, H. In *Metal Clusters in Catalysis*; Gates, B. C., Guczi, L., Knözinger, H., Eds.; Elsevier: Amsterdam, 1986; p 178.
(20) Weckhuysen, B. M. *Chem. Commun.* **2002**, 97.
(21) Xu, T.; Haw, J. F. *Top. Catal.* **1997**, *4*, 109.
(22) Haw, J. F. *Top. Catal.* **1999**, *8*, 81.
(23) Heald, S. M. In *X-Ray Absorption: Principles, Applications, Techniques of EXAFS, SEXAFS and XANES*; Koningsberger, D. C., Prins, R., Eds.; Wiley: New York, 1988; pp 108−112.
(24) Jentoft, R. E.; Deutsch, S. E.; Gates, B. C. *Rev. Sci. Instrum.* **1996**, *67*, 2111.
(25) Odzak, J. F.; Argo, A. M.; Lai, F. S.; Gates, B. C.; Pandya, K.; Feraria, L. *Rev. Sci. Instrum.* **2001**, *72*, 3943.
(26) Drake, I. J.; Liu, T. C. N.; Gilles, M.; Tyliszczak, T.; Kilcoyne, A. L. D.; Shuh, D. K.; Mathies, R. A.; Bell, A. T. *Rev. Sci. Instrum.* **2004**, *75*, 3242.
(27) Pettiti, I.; Gazzoli, D.; Inversi, M.; Valigi, M.; De Rossi, S.; Ferraris, G.; Porta, P.; Colonna, S. *J. Synchrotron Radiat.* **1999**, *6*, 1120.
(28) Huwe, H.; Fröba, M. *J. Synchrotron Radiat.* **2004**, *11*, 363.
(29) The spectroscopic and microscopic methods referred to here are for the most part well established and used in the investigation of catalysts.

Only a few details are included here to address the specific requirements of the applications to supported metal complexes and clusters. However, we emphasize that X-ray absorption spectroscopy is still a developing technique, which has been improving with the capabilities offered by synchrotrons. X-ray absorption spectroscopy is still less readily available to researchers than most of the other techniques described here, in part because of the need for specialized equipment for sample handling at a synchrotron and in part because of the challenges of data fitting. Analysis of EXAFS and XANES data is not entirely straightforward, requiring chemical insight in the choice of candidate structures. Therefore, to help readers develop an understanding of the X-ray absorption characterization methods discussed below, further details of this technique are provided in the Appendix.

(30) Koningsberger, D. C.; Mojet, B. L.; van Dorssen, G. E.; Ramaker, D. E. *Top. Catal.* **2000**, *10*, 143.
(31) Rehr, J. J.; Ankudinov, A. L. *Coord. Chem. Rev.* **2005**, *249*, 131.
(32) Ankudinov, A. L.; Ravel, B.; Rehr, J. J.; Conradson, S. D. *Phys. Rev. B* **1998**, *58*, 7565.
(33) Lee, P. A.; Citrin, P. H.; Eisenberger, P.; Kincaid, B. M. *Rev. Mod. Phys.* **1981**, *53*, 769.
(34) Sayers, D. E.; Stern, E. A.; Lytle, F. W. *Phys. Rev. Lett.* **1971**, *27*, 1204.
(35) Knözinger, H. In *Metal Clusters in Catalysis*; Gates, B. C., Guczi, L., Knözinger, H., Eds.; Elsevier: Amsterdam, 1986; pp 259−263.
(36) Brenner, A. In *Metal Clusters*; Moskovits, M., Ed.; Wiley: New York, 1986; pp 255−258.
(37) Bhirud, V. A.; Iddir, H.; Browning, N. D.; Gates, B. C. *J. Phys. Chem. B* **2005**, *109*, 12738.
(38) Sohlberg, K.; Rashkeev, S.; Borisevich, A. Y.; Pennycook, S. J.; Pantelides, S. T. *Chem. Phys. Chem.* **2004**, *5*, 1893.
(39) Bhirud, V. A.; Moses, M. J.; Blom, D. A.; Allard, L. F.; Aoki, T.; Mishina, S.; Narula, C. K.; Gates, B. C. *Microsc. Microanal.* **2005**, *11*, Supplement S02, 1574.
(40) Goellner, J. F.; Gates, B. C.; Vayssilov, G. N.; Rösch, N. *J. Am. Chem. Soc.* **2000**, *122*, 8056.
(41) IXS Standards and Criteria Committee *Error Reporting Recommendations: A Report of the Standards and Criteria Committee* 2000.
(42) Alexeev, O.; Gates, B. C. *Top. Catal.* **2000**, *10*, 273.
(43) Ramaker, D. E.; van Dorssen, G. E.; Mojet, B. L.; Koningsberger, D. C. *Top. Catal.* **2000**, *10*, 157.
(44) Ankudinov, A. L.; Rehr, J. J.; Low, J. J.; Bare, S. R. *Phys. Rev. Lett.* **2001**, *86*, 1642.
(45) Ankudinov, A. L.; Rehr, J. J.; Low, J. J.; Bare, S. R. *Top. Catal.* **2002**, *18*, 3.
(46) Ehresmann, J. O.; Kletnieks, P. W.; Liang, A. J.; Bhirud, V. A.; Bagatchenko, O. P.; Lee, E. J.; Klaric, M.; Gates, B. C.; Haw, J. F. *Angew. Chem., Int. Ed.* **2006**, *45*, 574.
(47) Kirlin, P. S.; van Zon, F. B. M.; Koningsberger, D. C.; Gates, B. C. *J. Phys. Chem.* **1990**, *94*, 8439.
(48) Kirlin, P. S.; Gates, B. C. *Nature* **1987**, *325*, 38.
(49) Kirlin, P. S.; Knözinger, H.; Gates, B. C. *J. Phys. Chem.* **1990**, *94*, 8451.
(50) Hu, A.; Neyman, K. M.; Staufer, M.; Belling, T.; Gates, B. C.; Rösch, N. *J. Am. Chem. Soc.* **1999**, *121*, 4522.
(51) Varela, M.; Lupini, A. R.; van Benthem, K.; Borisevich, A. Y.; Chisholm, M. F.; Shibata, N.; Abe, E.; Pennycook, S. J. *Annu. Rev. Mater. Res.* **2005**, *35*, 539.
(52) Bernal, S.; Botana, F. J.; Calvino, J. J.; López-Cartes, C.; Pérez-Omil, J. A.; Rodríguez-Izquierdo, J. M. *Ultramicroscopy* **1998**, *72*, 135.
(53) Fung, A. S.; Tooley, P. A.; Kelley, M. J.; Koningsberger, D. C.; Gates, B. C. *J. Phys. Chem.* **1991**, *95*, 225.
(54) Bhirud, V. A.; Uzun, A.; Lobo, R. J.; Gates, B. C. to be published.
(55) Bhirud, V. A.; Panjabi, G.; Salvi, S. N.; Phillips, B. L.; Gates, B. C. *Langmuir* **2004**, *20*, 6173.
(56) Scanning tunneling microscopy (STM) can also be applied to characterize the nuclearities of small supported metal clusters and can be used to resolve structures at the atomic level[57] and provide information about the heights of supported clusters, which is important for the elucidation of their three-dimensional structures. Thus, STM complements TEM and EXAFS spectroscopy. However, STM requires nearly flat surfaces, and applications of this technique to catalyst characterization are essentially restricted to single crystals. For example, STM has been used to image nearly uniform gold clusters formed by deposition of size-selected clusters from the gas phase onto TiO_2 (rutile); the images indicate that the clusters changed from two-dimensional to three-dimensional as the number of gold atoms per cluster increased from 2 to 8.[58]
(57) Besenbacher, F. *Rep. Prog. Phys.* **1996**, *59*, 1737.
(58) Tong, X.; Benz, L.; Kemper, P.; Metiu, H.; Bowers, M. T.; Buratto, S. K. *J. Am. Chem. Soc.* **2005**, *127*, 13516.
(59) Maloney, S. D.; van Zon, F. B. M.; Kelley, M. J.; Koningsberger, D. C.; Gates, B. C. *Catal. Lett.* **1990**, *5*, 161.
(60) Kawi, S.; Gates, B. C. *J. Phys. Chem.* **1995**, *99*, 8824.
(61) Alexeev, O.; Panjabi, G.; Gates, B. C. *J. Catal.* **1998**, *173*, 196.
(62) Li, F.; Gates, B. C. *J. Phys. Chem. B* **2003**, *107*, 11589.
(63) Goellner, J. F.; Guzman, J.; Gates, B. C. *J. Phys. Chem. B* **2002**, *106*, 1229.
(64) Maloney, S. D.; Kelly, M. J.; Koningsberger, D. C.; Gates, B. C. *J. Phys. Chem.* **1991**, *95*, 9406.
(65) Zhao, A.; Gates, B. C. *J. Am. Chem. Soc.* **1996**, *118*, 2458.
(66) Argo, A. M.; Odzak, J. F.; Gates, B. C. *J. Am. Chem. Soc.* **2003**, *125*, 7107.
(67) Labouriau, A.; Panjabi, G.; Enderle, B.; Pietrass, T.; Gates, B. C.; Earl, W. L.; Ott, K. C. *J. Am. Chem. Soc.* **1999**, *121*, 7674.
(68) Kawi, S.; Gates, B. C. *J. Chem. Soc., Chem. Commun.* **1991**, 994.
(69) Triantafillou, N. D.; Gates, B. C. *J. Phys. Chem.* **1994**, *98*, 8431.
(70) Weber, W. A.; Gates, B. C. *J. Phys. Chem. B* **1997**, *101*, 10423.
(71) Goellner, J. F.; Gates, B. C. *J. Phys. Chem. B* **2001**, *105*, 3269.
(72) Alexeev, O. S.; Panjabi, G.; Phillips, B. L.; Gates, B. C. *Langmuir* **2003**, *19*, 9494.
(73) Bhirud, V.; Goellner, J. F.; Argo, A. M.; Gates, B. C. *J. Phys. Chem. B* **2004**, *108*, 9752.
(74) Panjabi, G.; Argo, A. M.; Gates, B. C. *Chem. Eur. J.* **1999**, *5*, 2417.
(75) Argo, A. M.; Gates, B. C. *Langmuir* **2002**, *18*, 2152.
(76) Argo, A. M.; Odzak, J. F.; Lai, F. S.; Gates, B. C. *Nature* **2002**, *415*, 623.
(77) Argo, A. M.; Gates, B. C. *J. Phys. Chem. B* **2003**, *107*, 5519.
(78) Neylon, M. K.; Marshall, C. L.; Kropf, J. A. *J. Am. Chem. Soc.* **2002**, *124*, 5457.
(79) Marques, E. C.; Sandstrom, D. R.; Lytle, F. W.; Greegor, R. B. *J. Chem. Phys.* **1982**, *77*, 1027.
(80) Crozier, E. D.; Rehr, J. J.; Ingalls, R. In *X-ray Absorption: Principles, Applications, Techniques of EXAFS, SEXAFS and XANES*; Koningsberger, D. C., Prins, R., Eds.; Wiley: New York, 1988; p 373 ff.
(81) Hung, N. V.; Frahm, R. *Physica B* **1995**, *208/209*, 97.
(82) Hung, N. V.; Rehr, J. J. *Phys. Rev. B* **1997**, *56*, 43.
(83) Vayssilov, G. N.; Gates, B. C.; Rösch, N. *Angew. Chem., Int. Ed.* **2003**, *42*, 1391.
(84) Vayssilov, G. N.; Rösch, N. *Phys. Chem. Chem. Phys.* **2005**, *7*, 4019.
(85) Ferrari, A. M.; Neyman, K. M.; Mayer, M.; Staufer, M.; Gates, B. C.; Rösch, N. *J. Phys. Chem. B* **1999**, *103*, 5311.
(86) Goellner, J. F.; Neyman, K. M.; Mayer, M.; Nörtemann, F.; Gates, B. C.; Rösch, N.; *Langmuir* **2000**, *16*, 2736.
(87) Neyman, K.; Rösch, N.; Pacchioni, G. *Appl. Catal. A* **2000**, *191*, 3.
(88) Köster, A. M.; Calaminici, P.; Gómez, Z.; Reveles, U. In *Reviews of Modern Quantum Chemistry*; Sen, K. D., Ed.; World Scientific: Singapore, 2002; Vol. 2, p 1439 ff.
(89) Neyman, K. M.; Illas, F. *Catal. Today* **2005**, *105*, 2.
(90) Deeba, M.; Streusand, B. J.; Schrader, G. L.; Gates, B. C. *J. Catal.* **1981**, *69*, 218.
(91) Knözinger, H. In *Metal Clusters in Catalysis*; Gates, B. C., Guczi, L., Knözinger, H., Eds.; Elsevier: Amsterdam, 1986; pp 156−158.
(92) Mestl, G.; Triantafillou, N. D.; Knözinger, H.; Gates, B. C. *J. Phys. Chem.* **1993**, *97*, 666.
(93) Kortüm, G. *Reflexionsspektroskopie*; Springer: Berlin, 1969.
(94) Barth, R.; Gates, B. C.; Zhao, Y.; Knözinger, H.; Hulse, J. *J. Catal.* **1983**, *82*, 147.
(95) Tyles, D. R.; Levenson, R. A.; Gray, H. B. *J. Am. Chem. Soc.* **1978**, *100*, 7888.
(96) Shriver, D.; Atkins, P. *Inorganic Chemistry*, 3rd ed.; Freeman, W. H.: New York, 1999; pp 539−543.
(97) Bhaduri, S.; Mukesh, D. *Homogeneous Catalysis*; Wiley: New York, 2000; pp 13−15.
(98) Basset, J.-M.; Lefebvre, F.; Santini, C. *Coord. Chem. Rev.* **1998**, *178−180*, 1703.
(99) Guzman, J.; Gates, B. C. *J. Phys. Chem. B* **2003**, *107*, 2242.
(100) Guzman, J.; Gates, B. C. *Angew. Chem., Int. Ed.* **2003**, *42*, 690.
(101) Calla, J. T.; Davis, R. J. *J. Phys. Chem. B* **2005**, *109*, 2307.
(102) Guzman, J.; Gates, B. C. *J. Catal.* **2004**, *226*, 111.
(103) Fierro-Gonzalez, J. C.; Bhirud, V. A.; Gates, B. C. *Chem. Commun.* **2005**, 5275.
(104) Durham, P. J. In *X-Ray Absorption: Principles, Applications, Techniques of EXAFS, SEXAFS and XANES*; Koningsberger, D. C., Prins, R., Eds.; Wiley: New York, 1988; pp 53−57.
(105) Valencia, E.; Santarsiero, B. D.; Geib, S. J.; Rheingold, A. L.; Mayer, J. M. *J. Am. Chem. Soc.* **1987**, *109*, 6896.
(106) Cotton, F. A.; Diebold, M. P.; Roth, W. J. *J. Am. Chem. Soc.* **1987**, *109*, 2833.
(107) Babaian-Kibala, E.; Cotton, F. A.; Shang, M. *Inorg. Chem.* **1990**, *29*, 5148.
(108) Sokolov, M. N.; Fedin, V. P. *Coord. Chem. Rev.* **2004**, *248*, 925.
(109) Haruta, M.; Tsubota, S.; Kobayashi, T.; Kageyama, H.; Genet, M. J.; Delmon, B. *J. Catal.* **1993**, *144*, 175.
(110) Guzman, J.; Gates, B. C. *Langmuir* **2003**, *19*, 3897.

(111) Fierro-Gonzalez, J. C.; Gates, B. C. *J. Phys. Chem. B* **2005**, *109*, 7275.

(112) Fernández-García, M.; Márquez Alvarez, C.; Haller, G. L. *J. Phys. Chem.* **1995**, *99*, 12565.

(113) Bazin, D.; Rehr, J. J. *J. Phys. Chem. B* **2003**, *107*, 12398.

(114) For example, the sensitivity of Pt-L_{III}-edge XANES to local geometry and electronic structure of platinum clusters was investigated theoretically with the ab initio self-consistent FEFF8 code developed by the group of Rehr.[115,116] The calculations show that XANES can distinguish 2- and 3-dimensional shapes of small platinum clusters.[116] The calculated spectra show that the white-line intensity depends strongly on the size of a small cluster and becomes independent of cluster size for large clusters (estimated for Pt to consist of 13 or more atoms).[115,116] A limitation of the theoretical calculations based on the FEFF8 code that have been reported so far is the lack of a convincing representation of the support, which is typically modeled by considering only a few atoms of the oxide support close to the metal or a simplified model of a zeolite cage.[116−118] Moreover, in all the theoretical calculations carried out in attempts to consider the effect of the support on the XANES, it has been assumed that all the supported clusters are located at equivalent sites, which might be a significant oversimplification. More work is needed on the theory of XANES for interpretation and prediction of the spectra of samples containing extremely small structures on supports.

(115) Ankudinov, A. L.; Rehr, J. J.; Low, J. J.; Bare, S. R. *J. Synchrotron Radiat.* **2001**, *8*, 578.

(116) Ankudinov, A. L.; Rehr, J. J.; Low, J. J.; Bare, S. R. *J. Chem. Phys.* **2002**, *116*, 1911.

(117) Koningsberger, D. C.; Oudenhuijzen, M. K.; de Graaf, J.; van Bokhoven, J. A.; Ramaker, D. E. *J. Catal.* **2003**, *216*, 178.

(118) Ramaker, D. E.; Teliska, M.; Zhang, Y.; Stakheev, A. Yu.; Koningsberger, D. C. *Phys. Chem. Chem. Phys.* **2003**, *5*, 4492.

(119) Niemantsverdriet, J. W.; Delgass, W. N. *Top. Catal.* **1999**, *8*, 133.

(120) Kleimenov, E.; Bluhm, H.; Hävecker, M.; Knop-Gericke, A.; Pestryakov, A.; Teschner, D.; Lopez-Sanchez, J. A.; Bartley, J. K.; Hutchings, G. J.; Schlögl, R. *Surf. Sci.* **2005**, *575*, 181.

(121) Würz, R.; Rusu, M.; Schedel-Niedrig, Th.; Lux-Steiner, M. Ch.; Bluhm, H.; Hävecker, M.; Kleimenov, E.; Knop-Gericke, A.; Schlögl, R. *Surf. Sci.* **2005**, *580*, 80.

(122) Stievno, L.; Wagner, F. E. *AIP Conf. Proc.* **2004**, *765*, 3.

(123) Hercules, D. M.; Houalla, M.; Proctor, A.; Fiedor, J. N. *Anal. Chim. Acta* **1993**, *283*, 42.

(124) Cimino, A.; Gazzoli, D.; Valigi, M. *J. Electron Spectrosc. Relat. Phenom.* **1999**, *104*, 1.

(125) Venezia, A. M. *Catal. Today* **2003**, *77*, 359.

(126) Foley, H. C.; DeCanio, S. J.; Tau, K. D.; Chao, K. J.; Onuferko, J. H.; Dybowski, C.; Gates, B. C. *J. Am. Chem. Soc.* **1983**, *105*, 3074.

(127) Miessner, H.; Burkhardt, I.; Gutschick, D.; Zecchina, A.; Morterra, C.; Spoto, G. *J. Chem. Soc., Faraday Trans. 1* **1989**, *85*, 2113.

(128) Weber, W. A.; Gates, B. C. *Chem. Eur. J.* **1999**, *5*, 2899.

(129) Rao, L.-F.; Hwang, S.-J.; King, T. S.; Pruski, M. *J. Phys. Chem.* **1996**, *100*, 5668.

(130) Triantafillou, N. D.; Purnell, S. K.; Papile, C. J.; Chang, J.-R.; Gates, B. C. *Langmuir* **1994**, *10*, 4077.

(131) Kirlin, P. S.; DeThomas, F. A.; Bailey, J. W.; Gold, H. S.; Dybowski, C.; Gates, B. C. *J. Phys. Chem.* **1986**, *90*, 4882.

(132) Li, F.; Gates, B. C. *J. Phys. Chem. B* **2004**, *108*, 11259.

(133) Kawi, S.; Gates, B. C. *Inorg. Chem.* **1992**, *31*, 2939.

(134) Petroff Saint-Arroman, R.; Chabanas, M.; Baudouin, A.; Copéret, C.; Basset, J.-M.; Lesage, A.; Emsley, L. *J. Am. Chem. Soc.* **2001**, *123*, 3820.

(135) Chabanas, M.; Alessandra Quadrelli, E.; Fenet, B.; Copéret, C.; Thivolle-Cazat, J.; Basset, J.-M.; Lesage, A.; Emsley, L. *Angew. Chem., Int. Ed.* **2001**, *40*, 4493.

(136) Chabanas, M.; Baudouin, A.; Copéret, C.; Basset, J.-M.; Lukens, W.; Lesage, A.; Hediger, S.; Emsley, L. *J. Am. Chem. Soc.* **2003**, *125*, 492.

(137) Le Roux, E.; Chabanas, M.; Baudouin, A.; de Mallmann, A.; Copéret, C.; Alessandra Quadrelli, E.; Thivolle-Cazat, J.; Gasset, J.-M.; Lukens, W.; Lesage, A.; Emsley, L.; Sunley, G. J. *J. Am. Chem. Soc.* **2004**, *126*, 13391.

(138) Quignard, F.; Lecuyer, C.; Bougault, C.; Lefebvre, F.; Choplin, A.; Olivier, D.; Basset, J.-M. *Inorg. Chem.* **1992**, *31*, 928.

(139) Chabanas, M.; Baudouin, A.; Copéret, C.; Basset, J.-M. *J. Am. Chem. Soc.* **2001**, *123*, 2062.

(140) Corker, J.; Lefebvre, F.; Lécuyer, C.; Dufaud, V.; Quignard, F.; Choplin, A.; Evans, J.; Basset, J.-M. *Science* **1996**, *271*, 966.

(141) Vidal, V.; Theolier, A.; Thivolle-Cazat, J.; Basset, J.-M. *Science* **1997**, *276*, 99.

(142) Maury, O.; Lefort, L.; Vidal, V.; Thivolle-Cazat, J.; Basset, J.-M. *Angew. Chem., Int. Ed.* **1999**, *38*, 1952.

(143) Soulivong, D.; Copéret, C.; Thivolle-Cazat, J.; Basset, J.-M.; Maunders, B. M.; Pardy, R. B. A.; Sunley, G. J. *Angew. Chem., Int. Ed.* **2004**, *43*, 5366.

(144) Thieuleux, C.; Copéret, C.; Dufaud, V.; Marangelli, C.; Kuntz, E.; Basset, J.-M. *J. Mol. Catal. A* **2004**, *213*, 47.

(145) Vidal, V.; Théolier, A.; Thivolle-Cazat, J.; Basset, J.-M.; Corker, J. *J. Am. Chem. Soc.* **1996**, *118*, 4595.

(146) Rataboul, F.; Baudouin, A.; Thieuleux, C.; Veyre, L.; Copéret, C.; Thivolle-Cazat, J.; Basset, J.-M.; Lesage, A.; Emsley, L. *J. Am. Chem. Soc.* **2004**, *126*, 12541.

(147) Li, F.; Yu, P.; Hartl, M.; Daemen, L. L.; Eckert, J.; Gates, B. C., to be published.

(148) Dufaud, V.; Niccolai, G. P.; Thivolle-Cazat, J.; Basset, J.-M. *J. Am. Chem. Soc.* **1995**, *117*, 4288.

(149) Lefort, L.; Chabanas, M.; Maury, O.; Meunier, D.; Copéret, C.; Thivolle-Cazat, J.; Basset, J.-M. *J. Organomet. Chem.* **2000**, *593−594*, 96.

(150) Koningsberger, D. C.; Gates, B. C. *Catal. Lett.* **1992**, *14*, 271.

(151) Papile, C. J.; Gates, B. C. *Langmuir* **1992**, *8*, 74.

(152) Bruce, G. C.; Stobart, S. R. *Inorg. Chem.* **1988**, *27*, 3879.

(153) Nuber, B.; Oberdorfer, F.; Ziegler, M. L. *Acta Crystallorgr., Sect. B* **1981**, *37*, 2062.

(154) Fierro-Gonzalez, J. C.; Gates, B. C. *Langmuir* **2005**, *21*, 5693.

(155) Sanchez, A.; Abbet, S.; Heiz, U.; Schneider, W.-D.; Häkkinen, H.; Barnett, R. N.; Landman, U. *J. Phys. Chem. A* **1999**, *103*, 9573.

(156) Häkkinen, H.; Stéphane, A.; Sanchez, A.; Heiz, U.; Landman, U. *Angew. Chem., Int. Ed.* **2003**, *42*, 1297.

(157) Yoon, B.; Häkkinen, H.; Landman, U.; Wörz, A. S.; Antonietti, J.-M.; Abbet, S.; Judai, K.; Heiz, U. *Science* **2005**, *307*, 403.

(158) Fierro-Gonzalez, J. C.; Gates, B. C. *J. Phys. Chem. B* **2004**, *108*, 16999.

(159) Deutsch, S. E.; Chang, J.-R.; Gates, B. C. *Langmuir* **1993**, *9*, 1284.

(160) Duivenvoorden, F. B. M.; Koningsberger, D. C.; Uh, Y. S.; Gates, B. C. *J. Am. Chem. Soc.* **1986**, *108*, 6254.

(161) Asakura, K.; Yamada, M.; Iwasawa, Y.; Kuroda, H. *Chem. Lett.* **1985**, *4*, 511.

(162) Binsted, N.; Evans, J.; Neville Greaves, G.; Price, R. J. *Organometallics* **1989**, *8*, 613.

(163) Bhirud, V. A.; Ehresmann, J. O.; Kletnieks, P. W.; Haw, J. F.; Gates, B. C. *Langmuir* **2006**, *22*, 490.

(164) van't Blik, H. F. J.; van Zon, J. B. A. D.; Huizinga, T.; Vis, J. C.; Koningsberger, D. C.; Prins, R. *J. Am. Chem. Soc.* **1985**, *107*, 3139.

(165) Chang, J.-R.; Gron, L. U.; Honji, A.; Sanchez, K. M.; Gates, B. C. *J. Phys. Chem.* **1991**, *95*, 9944.

(166) Honji, A.; Gron, L. U.; Chang, J.-R.; Gates, B. C. *Langmuir* **1992**, *8*, 2715.

(167) Kawi, S.; Chang, J.-R.; Gates, B. C. *J. Phys. Chem.* **1993**, *97*, 5375.